Geoscience Frontiers 9 (2018) 689–714

HOSTED BY

Contents lists available at ScienceDirect

China University of Geosciences (Beijing)

Geoscience Frontiers

journal homepage: www.elsevier.com/locate/gsf

Research Paper

Highly refractory Archaean peridotite cumulates: Petrology and geochemistry of the Seqi Ultramafic Complex, SW Greenland

Kristoffer Szilas [a,*], Vincent van Hinsberg [b], Iain McDonald [c], Tomas Næraa [d], Hugh Rollinson [e], Jacob Adetunji [e], Dennis Bird [a]

[a] Department of Geological Sciences, Stanford University, 450 Serra Mall, Stanford, CA 94305, USA
[b] Department of Earth & Planetary Sciences, McGill University, Quebec, Canada
[c] Department of Geology, Lund University, Sölvegatan 12, 223 62 Lund, Sweden
[d] School of Earth and Ocean Sciences, Cardiff University, Main Building, Cardiff CF10 3AT, United Kingdom
[e] College of Science, University of Derby, Derby, DE22 1GB, UK

ARTICLE INFO

Article history:
Received 21 November 2016
Received in revised form
3 May 2017
Accepted 21 May 2017
Available online 6 June 2017
Handling Editor: Sohini Ganguly

Keywords:
North Atlantic Craton
Archaean
Dunite
Platinum-group elements
Ultra-depleted mantle
Fiskefjord

ABSTRACT

This paper investigates the petrogenesis of the Seqi Ultramafic Complex, which covers a total area of approximately 0.5 km^2. The ultramafic rocks are hosted by tonalitic orthogneiss of the ca. 3000 Ma Akia terrane with crosscutting granitoid sheets providing an absolute minimum age of 2978 ± 8 Ma for the Seqi Ultramafic Complex. The Seqi rocks represent a broad range of olivine-dominated plutonic rocks with varying modal amounts of chromite, orthopyroxene and amphibole, i.e. various types of dunite (*s.s.*), peridotite (*s.l.*), as well as chromitite. The Seqi Ultramafic Complex is characterised primarily by refractory dunite, with highly forsteritic olivine with core compositions having Mg# ranging from about 91 to 93. The overall high modal contents, as well as the specific compositions, of chromite rule out that these rocks represent a fragment of Earth's mantle. The occurrence of stratiform chromitite bands in peridotite, thin chromite layers in dunite and poikilitic orthopyroxene in peridotite instead supports the interpretation that the Seqi Ultramafic Complex represents the remnant of a fragmented layered complex or a magma conduit, which was subsequently broken up and entrained during the formation of the regional continental crust.

Integrating all of the characteristics of the Seqi Ultramafic Complex points to formation of these highly refractory peridotites from an extremely magnesian (Mg# ~ 80), near-anhydrous magma, as olivine-dominated cumulates with high modal contents of chromite. It is noted that the Seqi cumulates were derived from a mantle source by extreme degrees of partial melting (>40%). This mantle source could potentially represent the precursor for the sub-continental lithospheric mantle (SCLM) in this region, which has previously been shown to be ultra-depleted. The Seqi Ultramafic Complex, as well as similar peridotite bodies in the Fiskefjord region, may thus constitute the earliest cumulates that formed during the large-scale melting event(s), which resulted in the ultra-depleted cratonic keel under the North Atlantic Craton. Hence, a better understanding of such Archaean ultramafic complexes may provide constraints on the geodynamic setting of Earth's first continents and the corresponding SCLM.

1. Introduction

Precambrian ultramafic rocks, such as komatiites, peridotites and associated cumulate rocks are of economic importance for commodities including Ni, Cr and platinum-group elements (PGEs) (e.g., Naldrett, 1999; Maier, 2005; Groves and Beirlein, 2007; Begg et al., 2010). The vast majority of peridotite occurrences from the Archaean and Proterozoic Eons are of cumulate rather than mantle origin, and are commonly related to komatiitic lava flows, or plutonic layered intrusions and anorthosite complexes, as exemplified by the localities such as the Bushveld, Fiskenæsset, Mount Keith, Stillwater and Windimurra complexes (Myers, 1976; Cameron, 1978; Mathison and Ahmat, 1996; McCallum, 1996;

* Corresponding author. Present address: Geological Survey of Denmark and Greenland (GEUS), Øster Voldgade 10, DK-1350 Copenhagen K, Denmark.
E-mail addresses: szilas@stanford.edu, ksz@geus.dk (K. Szilas).
Peer-review under responsibility of China University of Geosciences (Beijing).

http://dx.doi.org/10.1016/j.gsf.2017.05.003

Maier, 2005; Rosengren et al., 2005). Indisputable mantle rocks of Archaean age are only known as relatively small xenoliths found in kimberlites and alkaline dykes in cratonic settings (e.g., Bernstein et al., 1998; Downes, 2001; Pearson et al., 2004). The origins of larger bodies of ultramafic rocks associated with Archaean greenstone belts, with postulated ophiolitic affinities, are more controversial (e.g., Kusky et al., 2001; Friend et al., 2002; Rollinson, 2007; Zhao et al., 2007; Friend and Nutman, 2010; Szilas et al., 2015a).

In the North Atlantic Craton of Greenland, the greenstone/supracrustal belts are all considered to be of suprasubduction zone affinity and may therefore represent ophiolitic analogues (Polat et al., 2011; Furnes et al., 2015). However, in every case where associated ultramafic units were investigated in detail, it was concluded that they represent olivine-dominated cumulates derived from the concomitant volcanic and gabbroic sequences by fractional crystallisation processes (Szilas et al., 2012a, 2014c, 2015a).

The Mesoarchaean amphibolite- to granulite-facies Akia terrane of southern West Greenland forms part of the North Atlantic Craton (Fig. 1). This terrane is dominated mainly by tonalitic orthogneiss, although amphibolite and associated peridotite enclaves are found sporadically as metre- to kilometre-sized inclusions throughout

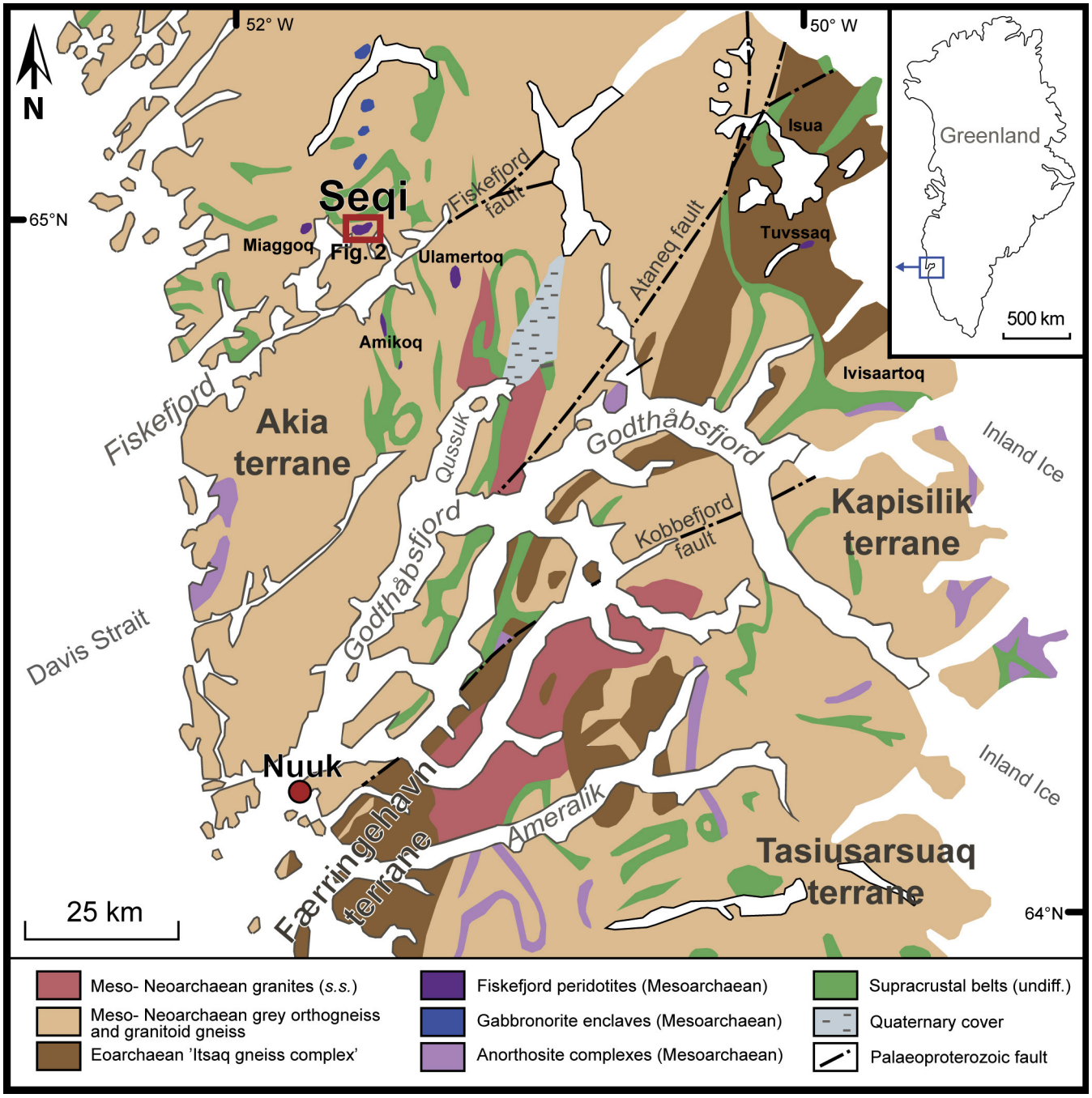

Figure 1. Simplified geological map of the Nuuk region with the Seqi Ultramafic Complex and several similar complexes along Fiskefjord marked in bold. The red square outlines the area of the detailed map of the Seqi Ultramafic Complex shown in Fig. 2. Red circle marks Nuuk, the capital of Greenland. The regional supracrustal belts range in age from Eo- to Neoarchaean. Regional mapping based on fieldwork by the Geological Survey of Denmark and Greenland (GEUS).

(Garde, 1997). The Seqi Ultramafic Complex represents one such peridotite complex within the Akia terrane and this is the subject of the present contribution. Its overall dimensions are approximately 500 m × 1000 m, which are distributed between two main peridotite bodies and several smaller inclusions (Fig. 2). With the location of the Seqi Ultramafic Complex at the coast, it is the most accessible of the larger peridotite occurrences along Fiskefjord. Despite the fact that the Seqi Ultramafic Complex was mined for industrial grade olivine from 2005–2010 by the Swedish company Minelco, there is so far only a single scientific publication about the Seqi peridotites with some preliminary geochemical data (Szilas et al., 2015b), and currently no accepted petrogenetic model exists for these highly refractory dunites. The internal company reports that have been released mainly deal with the technical aspects of mining (Christiansen, 1997, 1998; Mai, 1998; Dahl, 2004), and corresponding environmental monitoring of Fiskefjord (Asmund et al., 2009; Søndergaard et al., 2009). The preliminary study of Szilas et al. (2015b) proposed that the Seqi Ultramafic Complex may represent parts of a layered intrusion or magma conduit that could potentially be associated with the regionally abundant mafic volcanic and gabbroic rocks found throughout the Akia terrane as supracrustal belts.

The two main contrasting origins that can be envisioned for the Seqi peridotites, are tested against the new data presented in this work: (1) residual mantle fragment that formed by large degrees of melt-extraction, which left behind essentially pure dunite, as previously proposed for the formation of the sub-continental lithospheric mantle (SCLM) in this region (Bernstein et al., 1998, 2007), or (2) alternatively the peridotites represent ultramafic cumulates formed by olivine accumulation, which is also known from a range of different magma types in both extrusive (komatiite vs. picrite) and intrusive (Alaskan-type vs. anhydrous layered complexes) settings (e.g., Wager et al., 1960; Irvine, 1974, 1977; Burns, 1985; McBirney, 1996; Arndt et al., 2008). The first possibility would be important scientifically, because the only direct constraint on the Greenlandic Archaean mantle thus far are the relatively small xenoliths derived from SCLM. If, on the other hand, the Seqi peridotites formed by fractional crystallisation and mineral accumulation processes, this could have important economic implications given that Ni, Cr and PGE mineralisation can be hosted by ultramafic cumulates (Cawthorn, 1996; Zientek, 2012).

In the present study, a comprehensive geochemical data set is provided for dunite, peridotite and chromitite from the Seqi Ultramafic Complex, which are particularly well-exposed within the

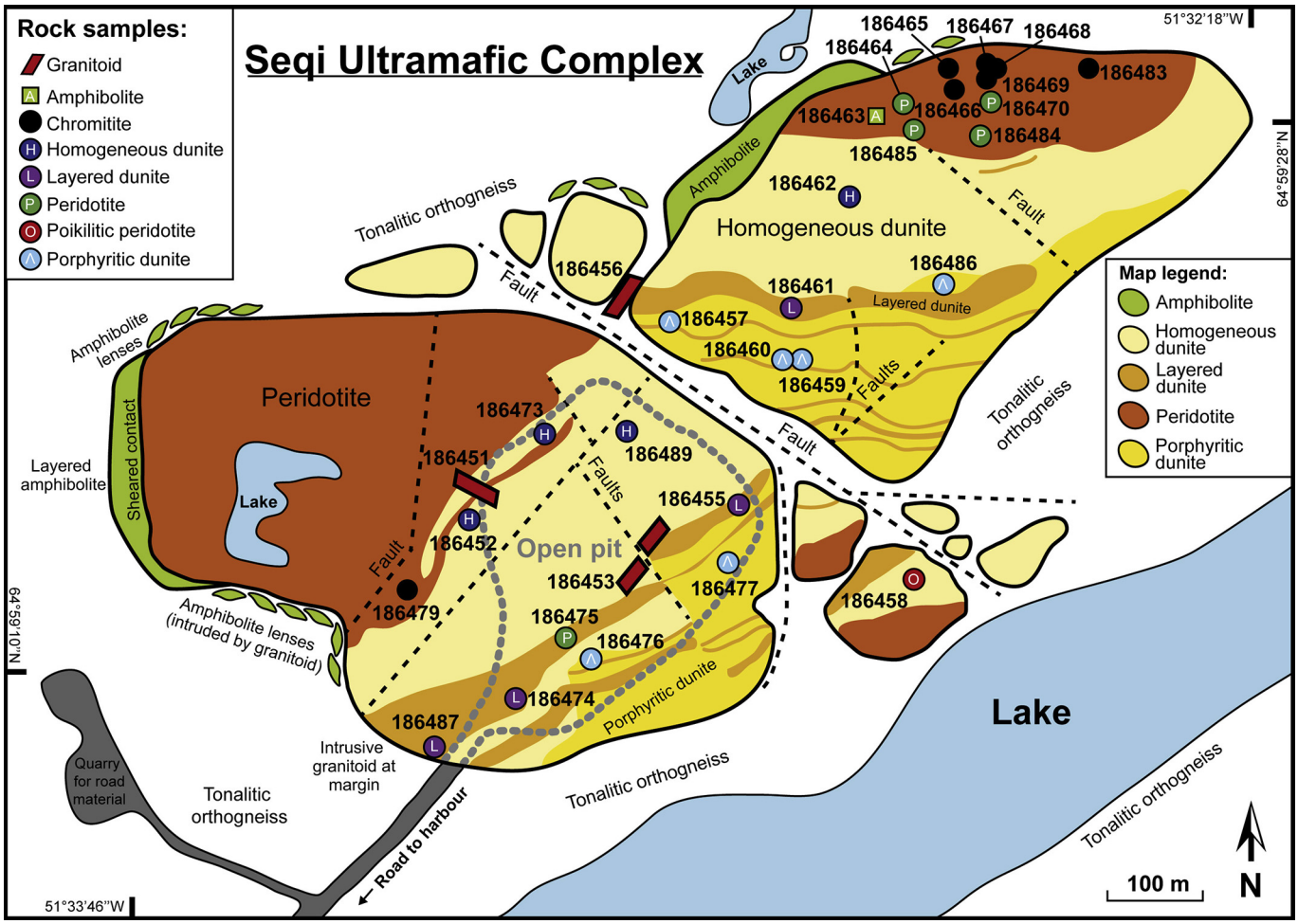

Figure 2. Detailed map of the Seqi Ultramafic Complex modified from Dahl (2004). The four main lithological units are shown, whereas chromitite bands and amphibolite veins are too small to outline at this scale and their presence is only marked by the sample positions. Note that we use peridotite (*sensu lato: s.l.*) in the broadest sense, and include all olivine-dominated (>40% modal olivine) plutonic rocks that are no strictly dunite (>90% modal olivine) (c.f. Streckeisen, 1976). The Seqi peridotites (*s.l.*) thus include various modal combinations of olivine–orthopyroxene–amphibole that do not outline any mapable systematics, but rather reflect mixtures of these minerals, which are mostly classified as amphibole–harzburgites. The Seqi Ultramafic Complex appears fragmented and its inclusion within the hosting tonalitic gneiss demonstrates that the latter was intrusive and thus postdates the formation of the ultramafic rocks. The outline of the open pit of the Seqi Olivine Mine in the western body of the Seqi Ultramafic Complex is marked with a stippled grey line.

Seqi Olivine Mine (Fig. 2). Field observations and petrography are presented, in combination with bulk-rock major, trace and platinum-group element data, as well as electron microprobe, LA-ICP-MS and Mössbauer mineral chemistry with the aim of producing a thorough petrological and geochemical characterisation of the different rock types found within the Seqi Ultramafic Complex. A petrogenetic model is developed based on these new data, and finally this ultramafic complex is placed into a regional context with potential implications for formation the sub-continental lithospheric mantle.

2. Regional geology

The Seqi Ultramafic Complex is located at Fiskefjord in the northern part of the Nuuk-region within Mesoarchaean tonalitic orthogneisses of the North Atlantic Craton (Fig. 1). It is worth noting at the outset that all of the Eo- to Neoarchaean supracrustal/greenstone belts within the North Atlantic Craton of Greenland are inferred to have formed in arc-related settings (Garde, 1997, 2007; Polat et al., 2002, 2007, 2011, 2015; Jenner et al., 2009; Szilas et al., 2011, 2012b, 2013a, 2017). It is debatable if any other tectonic setting is represented in this region due to the consistent arc-type geochemical signatures of the metabasalts (Jenner et al., 2014; Szilas et al., 2014a). Independent structural observations (Bridgwater et al., 1974; Hanmer and Greene, 2002; Kisters et al., 2012; Keulen et al., 2014; Polat et al., 2015) and the metamorphic evolution of the region (Dziggel et al., 2014; Arai et al., 2015; Dyck et al., 2015) also support the operation of horizontal accretionary processes and by inference uniformitarian plate tectonics, as being responsible for the formation of the North Atlantic Craton. In further support of this interpretation is the fact that, despite several decades of exploration and research, there are yet no komatiites (*s.s.*) reported from the North Atlantic Craton. Thus, it is relevant to study the petrogenesis of ultramafic rocks in this region to determine their origins and if they can be related to the metavolcanic rocks of the supracrustal/greenstone belts, which are mostly mafic to andesitic in composition. Finally, it is worth testing if any of these ultramafic rocks may represent mantle fragments.

The Seqi Ultramafic Complex is intruded by granitoid sheets (see field observations in Section 3 and zircon ages in Section 5.5), and thus it predates the ca. 3000 Ma regional continental crust-forming event of the Akia terrane. Similar occurrences of large (>100 m × 1000 m) peridotite enclaves and associated noritic rocks are found at the Miaggoq, Ulamertoq and Amikoq ultramafic complexes marked on Fig. 1, and several smaller occurrences are scattered along Fiskefjord (Garde, 1997; Kristensen, 2006; Szilas et al., 2015b).

The Nuuk region consists of several discrete crustal terranes, with the oldest being the over 3600 Ma Itsaq gneiss complex (Nutman et al., 1996) and the youngest being the ca. 2850 Ma Tasiusarsuaq terrane (Kolb et al., 2012). The majority of the crust is comprised of tonalite–trondhjemite–granodiorite (TTG) suite orthogneisses, but anorthosite complexes, metavolcanic and metasedimentary lithological units are also present as supracrustal/greenstone belts (Polat et al., 2002; Szilas et al., 2014b, 2015a, 2016a).

These different terranes experienced distinct tectono-magmatic evolution, but were ultimately amalgamated during the Neoarchaean (Friend and Nutman, 2005; Nutman and Friend, 2007). Peridotite bodies are also present within the Eoarchaean Itsaq gneiss complex, but these are generally not as extensive as those of the Mesoarchaean Akia terrane; and the former appear to be associated with fragmented anorthosite complexes and supracrustal belts. Thus, the peridotites of the Itsaq and Akia terranes appear to be of different ages and potentially have different petrogenetic origins (Bennett et al., 2002; Friend et al., 2002; Rollinson et al., 2002; Rollinson, 2007).

A recent overview of the igneous and metamorphic history of the Akia terrane was presented by Garde et al. (2015). Some of the main geological features relevant for understanding the Fiskefjord region peridotites are outlined in the following. The regional tonalite–trondhjemite–granodiorite (TTG) suite orthogneisses of the Akia terrane, which host the Seqi Ultramafic Complex, have been dated by U–Pb isotopes in zircon at ca. 3050–2975 Ma (Garde, 1997, 2007; Garde et al., 2015), although subordinate dioritic gneisses with magmatic ages of about 3200 Ma are also present (Garde, 1997). Supracrustal rocks (mainly tholeiitic metabasalt) form enclaves and coherent belts within the Akia terrane. These metavolcanic rocks have an age of ca. 3070 Ma, based on magmatic zircon extracted from volcano-sedimentary schist within the basaltic to andesitic Qussuk–Bjørneøen supracrustal sequence (Garde, 2007). The Akia terrane experienced late-tectonic granulite-facies metamorphism with local retrogression to amphibolite-facies at 2995–2975 Ma. Re-crystallisation of zircon, synkinematic intrusion of granite sheets, and isoclinal folding of the older diorites and early amphibolites was associated with this event (Garde, 1997, 2007; Garde et al., 2012, 2015).

3. Field observations and petrographical features

Representative samples were taken in 2013 in order to characterize the different rock units that comprises the Seqi Ultramafic Complex. Fig. 3 presents key field observations from the Seqi Ultramafic Complex, with additional field photos given in the supplementary Appendix A. The latter figures are given the prefix 'A' when referred to in the main text.

The present work focuses on dunites (*s.s.*), peridotites (*s.l.*), and the chromitite of the Seqi Ultramafic Complex. Amphibolite domains, reaction rims and veins are not studied in detail, as these represent minor components of the Seqi Ultramafic Complex and are likely of metasomatic/secondary nature, whereas the aim of the present study is to investigate the primary igneous petrogenesis. As will be shown in Section 5.3, the oxides are generally Cr–Al-rich spinel and thus, in the following discussion, spinel and chromite is used interchangeable, whereas it will be specified when secondary Cr-magnetite is present. The local rock classification for Seqi of Dahl (2004) is adopted here, which defines the following lithological units: homogeneous dunite, layered dunite, porphyritic dunite, poikilitic dunite (here revised to peridotite), peridotite, chromitite and amphibolite (Fig. 3). All of these rocks have been metamorphosed at upper amphibolite- to granulite facies conditions and their textures are mostly granoblastic (Fig. 4), with the exception of peculiar euhedral olivine crystals found in the porphyritic dunite (Fig. 3b). Note that we use the term 'peridotite' (*s.l.*) in its broadest sense to include olivine-dominated (>40%) plutonic rocks that also contain various combinations of orthopyroxene and amphibole. We thus use the peridotite definition of Streckeisen (1973, 1976) and Le Maitre et al. (2005) to include plutonic ultramafic rocks with over 40% modal olivine with any combination of orthopyroxene and amphibole regardless of origin (pyroxene–amphibole–peridotite or amphibole–harzburgite *sensu stricto*). The term 'dunite' is used for plutonic ultramafic rocks with more than 90% modal olivine, although this rock type is also a peridotite broadly speaking. For practical reasons, we thus simply distinguish between different types of pure dunite (*s.s.*) versus orthopyroxene–amphibole-bearing peridotite (*s.l.*) within the Seqi Ultramafic Complex.

Homogeneous dunite is dominated by olivine (up to 99 vol.%) and spinel typically constitutes 1–3 vol.% of the rock. Retrogression of chromite to magnetite and later to chlorite is common (Fig. 5)

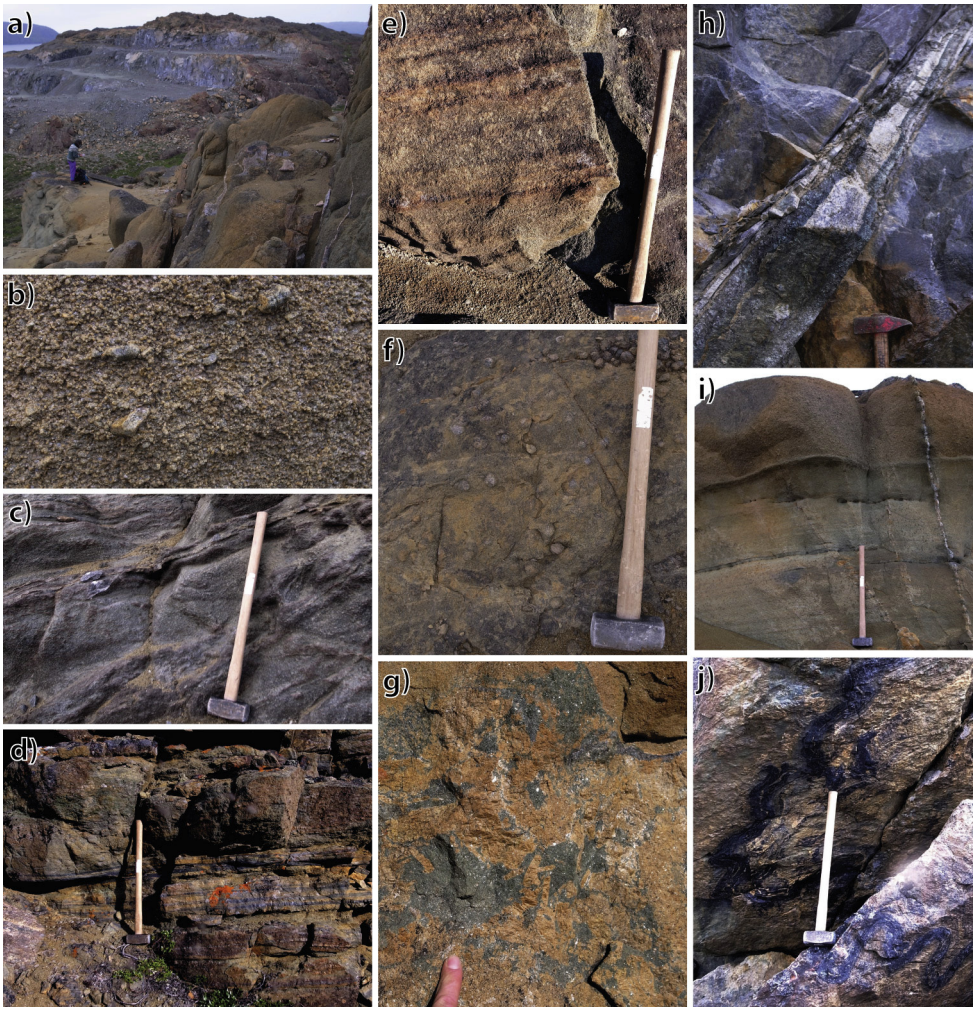

Figure 3. Field observations from the Seqi Ultramafic Complex. (a) Overview of the open pit of the Seqi Olivine Mine exposing walls of homogeneous dunite, which was the main ore during the operation of the mine. (b) Porphyritic dunite with showing euhedral olivine crystals up to about 2 cm long. (c) Peridotite with minor amounts of amphibole present interstitially. (d) Chromitite forming cm-thick stratiform layers in orthopyroxene-rich peridotite. (e) Layered dunite showing small ridges on the weathered surface where the modal content of chromite is elevated. (f) Poikilitic peridotite with round orthopyroxene oikocrysts up to 5 cm across. (g) Peridotite with green amphibole (tremolite) in coarse dunite ± orthopyroxene. Note the brecciated nature of the dunite within the amphibole domain (finger for scale). (h) Intrusive tonalitic sheet (sample 186451) showing strong reaction with the hosting homogeneous dunite. Zircon from this rock was dated at 2963 ± 6 Ma by LA-ICP-MS (see Section 5.5). (i) Amphibole and talc veins cut apparent layering in porphyritic dunite. Note the coarse grain size of the upper dunite unit in comparison with the lower. (j) Tightly folded chromitite layer in the NE part of the Seqi Ultramafic Complex. The head of the hammer that is used for scale in the above photographs is about 20 cm wide. Additional field photographs are presented in Appendix A.

and this causes the rock to easily disintegrate, yielding a pure olivine sand. Metamorphic phlogopite and amphibole is also present in the homogeneous dunite, but these minerals usually constitute less than 1 vol.% of the homogeneous dunite unit. Dahl (2004) reported rhythmic layering and crossbedding of orthopyroxene in the homogeneous dunite, which is a feature that was not observed in 2013 during the fieldwork carried out for the present work, although likely the result of excavation of the outcrop by mining.

Layered dunite is defined in the field by visible subparallel layering outlined by abundant chromite in regular horizons (Fig. 3e). Chromite typically forms a network of interlocking interstitial spinel, which gives a mesh-texture on weathered surfaces where olivine is lost (Fig. A13 in Appendix A). The chromite is also retrogressed locally to magnetite and chlorite; although not to the same extent as in the homogeneous dunite. Chromite is estimated to comprise less than 5 vol.% in the layered dunite, however, locally it may reach levels up to 12 vol.%.

Porphyritic dunite is characterized by coarse olivine with grain sizes up to about 0.5 cm and it may locally contain larger (up to 3 cm) euhedral olivine crystals (Fig. 3b). Chromite generally has as little abundance in this unit as in the homogeneous dunite with typically less than 2 vol.%.

Poikilitic peridotite is found only at one locality in the SE corner of the Seqi Ultramafic Complex (Fig. 2). It consists of dunite with coarse orthopyroxene oikocrysts up to 5 cm across, that readily weather out of the rock as seen in Fig. 3f. These orthopyroxene oikocrysts are commonly single crystals that overgrow olivine, chromite and amphibole, but orthopyroxene is also present as smaller grains throughout the matrix of this rock (Figs. 4 and 5). Orthopyroxene comprises up to 40 vol.% of this rock type and it is essentially harzburgitic.

Peridotite is a broadly defined unit which consists of various combinations of olivine, chromite, orthopyroxene and amphibole. The mineralogical variations of the Seqi peridotites (*sensu lato*) do not outline any mappable systematics, but rather reflect mixtures of these particular minerals. The strict term of this unit would thus be pyroxene–amphibole–peridotite or amphibole–harzburgite, but we use the term 'peridotite' (*s.l.*) throughout this paper to simplify the nomenclature. This unit locally has a large content of

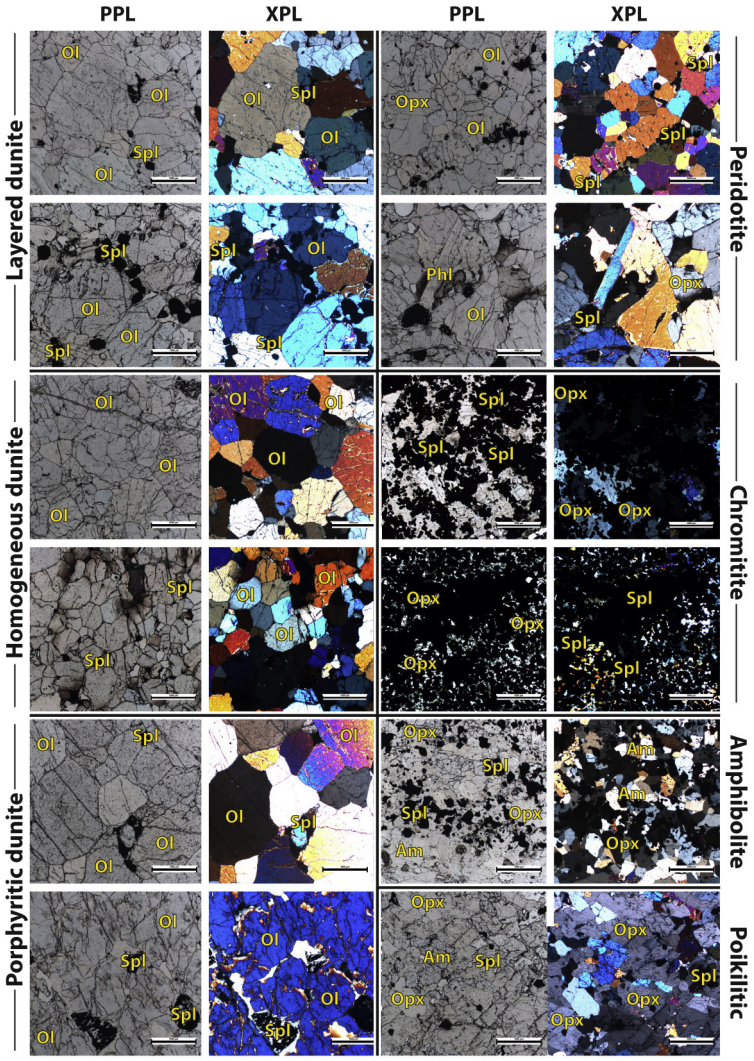

Figure 4. Representative polarized light microscopy photographs of the various lithological units found in the Seqi Ultramafic Complex. Each set shows plane polarized light (PPL) on the left and crossed polarized light (XPL) on the right. The scale bar in each lower right corner represents 1000 μm (1 mm) in all frames. The following mineral abbreviations are used: amphibole (Am), olivine (Ol), orthopyroxene (Opx), phlogopite (Phl) and spinel (Spl). See Section 3 for a detailed petrographic description of the each of the rock types. Additional microscope photographs are presented in Appendix B.

green amphibole (Fig. 3c), which is associated with abundant chromitite bands at the northern margin of the eastern enclave (Fig. 2).

Chromitite is found as cm-wide bands (up to 25 cm thick) within the peridotite unit and it is usually exclusively associated with interstitial orthopyroxene and has rather sharp transitions into surrounding olivine-rich domains (Figs. 4 and 5). Although chromitite mainly occurs as subparallel layers, it is locally strongly folded, resembling slump structures with buckling and breaking of the individual bands (Fig. 3j).

Amphibolite is represented by a single sample (186463) in the present data set for the Seqi Ultramafic Complex. This sample contains abundant ilmenite, which is phase that is not found in any of the other studied rock units in the Seqi Ultramafic Complex. The bulk-rock and mineral chemistry of the amphibolite sample is distinctly different from the rest of the studied rocks (Section 5). This particular amphibolite sample is from an amphibole-rich domain within the peridotite unit (see position in Fig. 2). Similar amphibole patches and veins are found throughout the peridotite unit and in association with infiltrating felsic dykes and veinlets derived from the granitoid host rock surrounding the Seqi Ultramafic Complex. Such amphibole veins thus appear to be of secondary/metasomatic origin. Layered amphibolites and smaller lenses of hornblendite are also present along the western and northern margins of the main peridotite complex. Note that these amphibolites have not been studied in detail, because the focus in the present work is on the various types of dunite and peridotite that comprise the Seqi Ultramafic Complex. It is possible, however, that the layered amphibolites may form a continuation of the olivine-dominated sequence, although their contact was observed to be strongly sheared in the western part of the ultramafic complex. No clinopyroxene has been observed in any of the rocks that were studied in the present work, although it could be argued that any clinopyroxene would have been transformed to amphibole during the metamorphic evolution of the Seqi Ultramafic Complex (see Section 5.7).

Granitoid rocks intruding the Seqi Ultramafic Complex were sampled for U–Pb zircon dating in order to constrain the minimum age of the ultramafic rocks (Section 5.5). Sample 186451 represents a 20 cm wide felsic intrusive sheet with a strike of 156° and a dip of 80°W. This sheet is fine grained and tonalitic in composition and it cuts the homogeneous dunite along a brittle

fracture. The felsic sheet has a ~3 cm reaction zone on either side consisting of chlorite, amphibole and talc. Sample 186453 is from a 1.5 m wide NE–SW trending (40°/65°SE) pegmatite sheet that intrudes the homogeneous dunite (Fig. A5 in Appendix A). It has a thick (20 cm) biotite-rich reaction zone at the contact to the homogeneous dunite. Sample 186456 is from the regional tonalitic orthogneiss that separates the two main ultramafic blocks of the Seqi Ultramafic Complex. In the field, it is not apparent if this orthogneiss has an originally intrusive or tectonic/structural contact with the Seqi Ultramafic Complex. However, several dunite enclaves are present within the orthogneiss surrounding the two main ultramafic bodies (Fig. 2), so it appears most likely that these are dismembered fragments of Seqi Ultramafic Complex that were entrained in the granitoids during the formation of the regional continental crust.

4. Methods

4.1. Bulk-rock major and trace element analysis

The ultramafic samples from the Seqi Ultramafic Complex selected for bulk-rock major and trace element analysis were cut into smaller pieces by diamond saw to avoid weathered surfaces. One part for XRF analysis was ground in a tungsten carbide mill. Peridotites require a quartz dilution for XRF, because the elevated Mg can cause crystallisation in the glass bead. Therefore, a separate aliquot was prepared for ICP-MS that was ground in a steel mill, which adds no contamination for the elements analysed by the ICP-MS.

Bulk-rock major and trace element data were acquired from the geochemical laboratory at Washington State University (WSU). The procedures involve flux-fusing of rock powders followed by standard XRF and ICP-MS methods. Any contamination from the Li-tetraborate flux was corrected for by a blank subtraction. The full analytical procedures are described on WSU's website and the reader is referred to this for the method details (WSU, 2016).

Table S1 in the supplementary material presents the major and trace element data, and includes measurements of several international standards, as well as estimates for precision and detection limits during the analysis. The XRF data have detection limits of around 20 ppm, and the ICP-MS analysis accurately measured most trace elements down to around 0.5 ppm. The software GCDKit of Janošek et al. (2006) was used for plotting the data. Supplementary geochemical diagrams are presented in Appendix D and are referred to with the prefix 'D' in the following sections.

4.2. Bulk-rock platinum-group element analysis

Platinum-group element (PGE) and Au data were obtained at Cardiff University, UK. Rock samples for PGE analysis were first cut into smaller pieces by diamond saw and the surfaces were polished with sand paper to avoid any risk of metal contamination from the saw. Sample powders for these analyses were milled in a ceramic shatter box to avoid metal contamination.

PGE and Au analysis was carried out by Ni-sulphide fire assay pre-concentration of 15 g sample material, followed by Te co-precipitation and measurement by ICP-MS. A full description of the instrumentation and analytical procedures are given in Huber et al. (2001) and McDonald and Viljoen (2013). Accuracy for whole-rock PGE and Au was constrained by analysis of the certified international reference materials SARM-64, TDB1 and WPR1, and the precision was estimated by repeat analysis of a sub-set of samples. PGE data obtained on samples from the Seqi Ultramafic Complex and the standards are provided in Table S2 in the supplementary material.

4.3. Electron microprobe mineral analysis

Electron microprobe analysis (EMPA) of the different mineral phases was conducted at Stanford University using a JEOL JXA-8230 with operating conditions of 15 kV, 20 nA, and a 2 μm spot size. Counting times were 20 s on peaks and 10 s on backgrounds. Mineral standards were measured at regular interval in each session to verify the accuracy of the analyses. The reader is referred to the supplementary Table S3 for the full electron microprobe data set obtained on samples from the Seqi Ultramafic Complex.

4.4. In situ trace element mineral analysis

In situ LA-ICP-MS measurements of trace elements in minerals were conducted at McGill University (Montreal, Canada) using a NewWave 213 nm Nd-YAG laser coupled to a Thermo Finnigan iCAP Q ICP-MS. Material was sampled in 80 μm wide and up to 2 mm long troughs, or 80 μm spots for zoned minerals, at 10 Hz repetition rate and a fluence of approximately 7.5 J/cm^2. The sample material was transported to the ICP-MS in a 800 mL/min He flow, which was mixed with Ar prior to injection into the plasma. The elements were split into a low-mass and a high-mass set and analysed in parallel lines or adjacent spots. Mineral analyses were bracketed by NIST SRM 610, and reference materials BCR-2G and GSD-1G were analysed to determine accuracy. All major elements were analysed in the low-mass set and data were normalised to the respective mineral formulae. The high-mass data set was normalised to Mg concentrations of equivalent low-mass data. Table S4 in the supplementary material presents the *in situ* LA-ICP-MS trace element data for various minerals from the Seqi Ultramafic Complex.

4.5. Zircon U–Pb isotope data

In situ LA-ICP-MS measurement of U–Pb isotopes in zircon was conducted at the Geological Survey of Denmark and Greenland (GEUS). Separation of zircon was done by crushing rock samples, which were then sieved at a mesh size of 300 μm. The heavy minerals were separated by panning. Magnetic minerals were removed from the heavy mineral concentrate using a hand magnet. Zircon grains were hand-picked from the final heavy mineral separate and were cast into epoxy resin and polished to expose a central cross-section of each grain. Back scattered electron (BSE) imaging was applied to reveal internal structures (Fig. 6), and energy dispersive spectroscopy (EDS) was applied to determine inclusion chemistry. BSE and EDS were carried out on a PHILIPS XL 40 SEM at GEUS.

The data were acquired on a Thermo Scientific Element2 magnetic mass spectrometer coupled to a NewWave UP213 laser ablation system, following the procedures outlined by Gerdes and Zeh (2006) and Frei and Gerdes (2009). Standard bracketing was done by analysing the Geostandard zircon GJ1 (Jackson et al., 2004). Analytical sessions were started with six measurements of the standard, followed by cycles of ten unknowns and three standard measurements. The laser was operated with a 25 μm spot size at a repetition rate of 10 Hz with a nominal energy output of 45–50% of the maximum laser intensity, corresponding to laser energy of about 0.025 mJ per pulse and a laser fluence of about 3 J/cm^2. For each analysis, the first 30 s were used to measure the gas blank (background), followed by 30 s of ablation and 20 s of washout time. Helium gas was used to flush the sample cell and was mixed downstream with the Ar sample gas before entering the plasma of the mass spectrometer. Measured masses were: ^{202}Hg, ^{204}(Pb + Hg), ^{206}Pb, ^{207}Pb, ^{208}Pb, ^{232}Th, ^{235}U and ^{238}U. The mass of ^{202}Hg was measured to monitor the ^{204}Hg isobaric interference on ^{204}Pb.

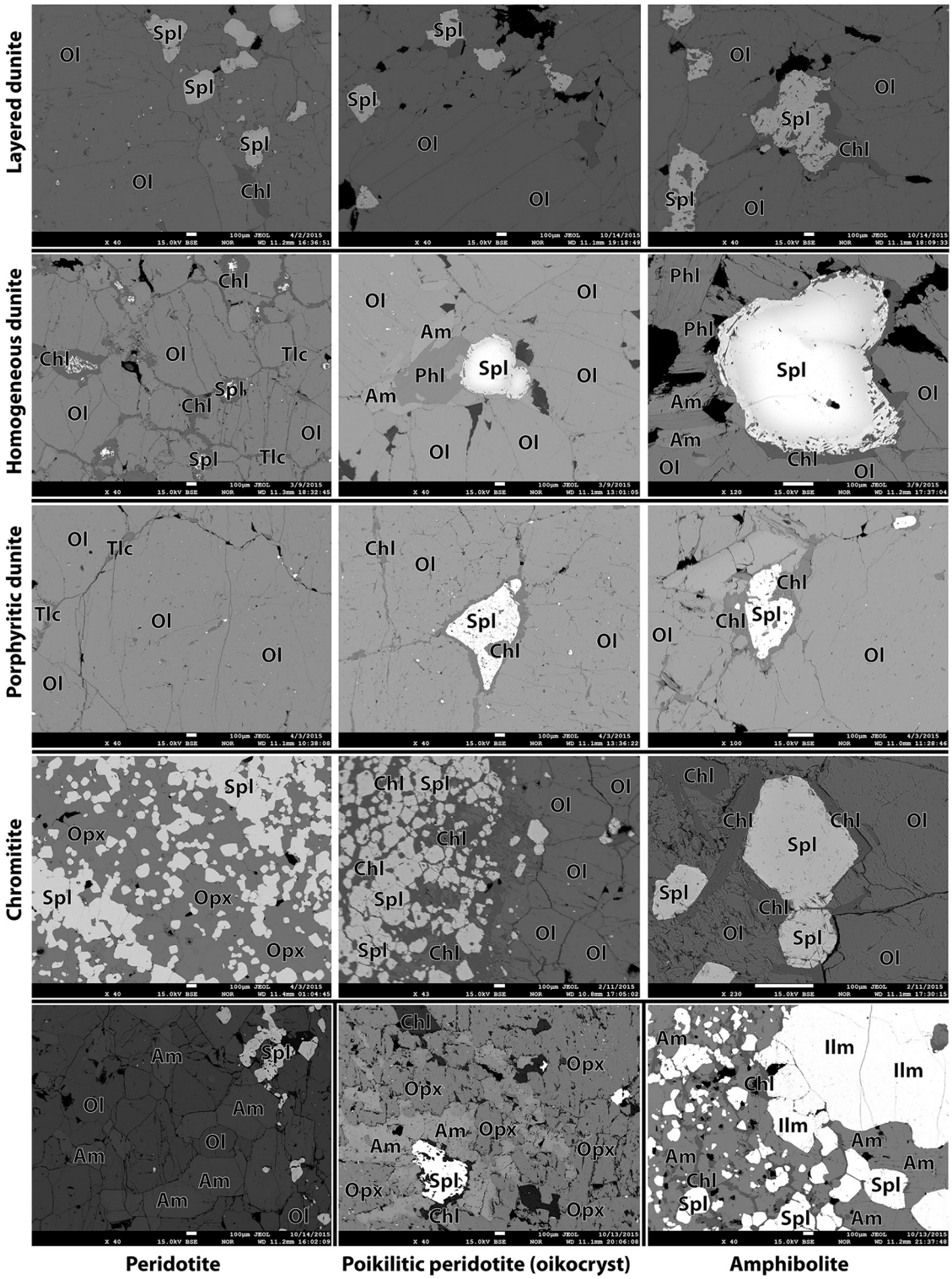

Figure 5. Back scattered electron (BSE) images (by EMPA) of the various rock units found in the Seqi Ultramafic Complex. Note that the first four horizontal panels are each for a single rock type, whereas the lower panel is for three different rock types. The following mineral abbreviations are used: amphibole (Am), chlorite (Chl), ilmenite (Ilm), olivine (Ol), orthopyroxene (Opx), phlogopite (Phl), spinel (Spl) and talc (Tlc). Additional BSE images are presented in Appendix C.

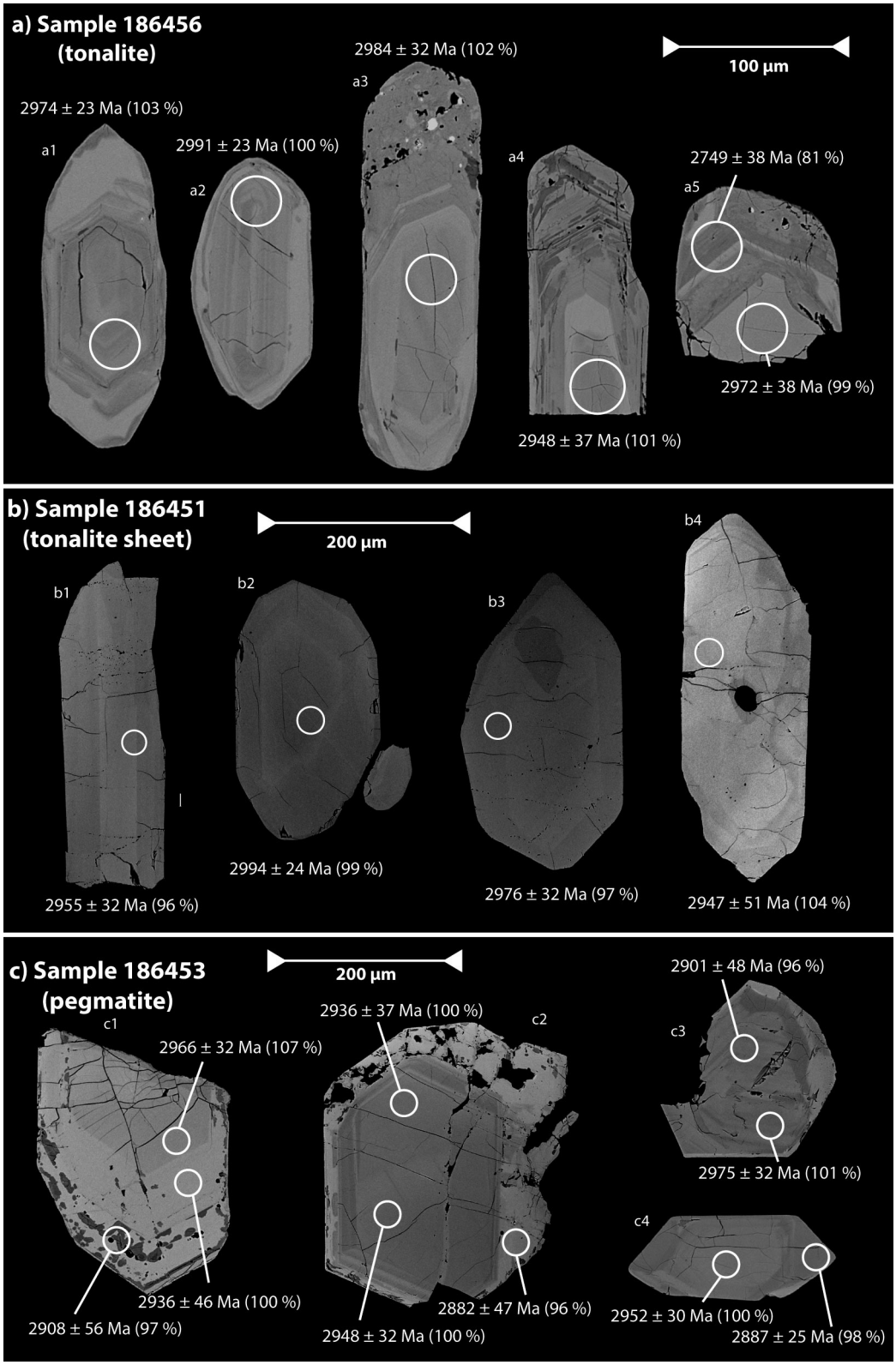

Figure 6. Back-scattered electron (BSE) images (by SEM) of representative zircon grains showing magmatic textures with internal zoning. Spot positions are marked together with their $^{207}Pb/^{206}Pb$ age (2σ error) and their concordance is indicated in parenthesis.The sample positions are indicated on the map in Fig. 2. (a) Sample 186456 is part of the regional orthogneiss that fragmented the Seqi Ultramafic Complex. (b) Sample 186451 is from an intrusive tonalitic (Fig. 3h) in the homogeneous dunite, which as a significant reaction rim consisting of mainly chlorite and amphibole. (c) Sample 186453 is from a NE–SW trending granitoid pegmatite (Fig. A5 in Appendix A).

Data reduction was performed using the Iolite software package (Paton et al., 2011). Data processing includes: (1) baseline corrections; (2) calculating a down-hole U–Th–Pb fractionation correction, and (3) applying a session-wide fractionation and instrumental drift corrections. The VizualAge data reduction scheme within Iolite was used to process 'live Concordia' diagrams (Petrus and Kamber, 2012). Isoplot 4.15 (Ludwig, 2012) was used for plotting data and for age calculations. See supplementary Table S5 for all of the U–Pb isotope data.

4.6. Mössbauer spectroscopy of chromitite

Mineral separates for Mössbauer spectroscopic analysis were prepared by first hammering the chromitite samples into progressively smaller fragments inside plastic bags shielded by paper to avoid any contamination with metal fragments from the hammer or plate. The rock grains were then split by nylon mesh sieves to <500 μm and 500–700 μm size fractions, and the latter was hand-picked for clean mineral separates consisting only of chromite.

Optical examinations of the samples show minute amounts of opaque phases (magnetite) at the grain boundaries, which could be magnetically separated after crushing the sample to a fine powder under acetone. Samples 186479, 186479b (replica) and 186466b have inter-grown minute crystals of chromite and a non-magnetic mineral, likely orthopyroxene, which could not be separated cleanly despite many repeats of hand-picking under the optical microscope.

^{57}Fe Mössbauer spectroscopic measurements were made on the samples (absorbers), each prepared from ~60 mg of the sample, mixed with boron nitride as a binder. The mixture was spread uniformly over an area of ~1.8 cm^2, and pressed into a pellet. The spectrometer uses a 25 mCi ^{57}Co in Rhodium matrix source mounted on a constant-acceleration transducer operated in a triangular mode in a velocity range, ±6 mm/s. The Doppler energies from the 14.4 keV γ-rays were detected with a $YAlO_3$:Ce scintillation counter. The data was recorded in 1024 channels, which cover twice the Doppler velocity range. Spectra were calibrated with a natural α-Fe foil and all peak positions reported with respect to the centroid shift (CS) of the natural α-Fe. MossA1.01a, a computer program developed by Prescher et al. (2012) utilizing a full transmission integral with a normalised Lorentzian source line-shape, was used to fit the Lorentzian lines of the folded data. The best fits to the data were obtained by reduced χ^2 criteria. The oxidation states of Fe-ions are then characterized by the centroid shift and the site occupancy determined by the quadrupole splitting (QS).

The uncertainties were calculated using the covariance matrix. Estimated uncertainties for CS, QS and full width at half maximum (FWHM) are ±0.020, ±0.030 and ±0.025 mm/s, respectively and less than ±2% absolute for absorption areas. A correction for the difference between the recoil-free fractions at room temperature for Fe^{2+} and Fe^{3+} in the tetrahedral and octahedral sites, respectively, was applied (Quintiliani, 2005). The criterion for identification of Fe-cation sites was based on the relative centroid shift values, following previous reports by Pal et al. (1994), Rais et al. (2003) and Rollinson et al. (2012) as $[\delta Fe^{3+}A] < [\delta Fe^{3+}B] < [\delta Fe^{2+}A] < [\delta Fe^{2+}B]$. The model was also found to be appropriate in Mössbauer spectroscopic investigation of Fe-cations distribution in natural chromites at different stages of oxidation (Pal et al., 1994).

In this study, several fitting models were tested to determine those that could be used with minimum constraints. To achieve this, four models were adopted: (1) $3Fe^{2+}(A) + 1Fe^{3+}(B)$ applied to two samples; (2) $2Fe^{2+}(A) + 1Fe^{3+}(B)$ applied to two samples; (3) $Fe^{2+}(A) + Fe^{2+}(B) + 2Fe^{3+}(B)$ applied to one sample. For this model, the quadrupole-splitting associated with the Fe^{2+} and Fe^{3+} ions are distinguished by $[\Delta qFe^{2+}B] < [\Delta qFe^{3+}B]$. (4) $1Fe^{2+}(A) + 2Fe^{3+}(B)$ model was applied to one sample. For the samples with inter-grown crystals, their $Fe^{3+}/\Sigma Fe$ ratios were only calculated from the absorption areas of chromite doublets of the sample spectra. The Mφssbauer data for the Seqi chromitite samples are provided in Table S6 in the supplementary material.

5. Results

5.1. Bulk-rock major and trace element data

The main bulk-rock geochemical characteristics of the different rock types in the Seqi Ultramafic Complex are briefly outlined here. The Seqi rocks are comparable to the regional Fiskefjord peridotites that were documented by Szilas et al. (2015b), however the Seqi dunites represent the most refractory components of this suite, as seen in Fig. 7. Bulk-rock mg# (given as molar Mg/[Mg + ΣFe] × 100%) assumes all iron to be divalent due to the olivine-rich nature of these rocks. Note that in this work we distinguish between bulk-rock 'mg#' (which uses ΣFe) and mineral 'Mg#' (which uses Fe^{2+} only). All of the data have been recalculated on a volatile-free basis, although loss on ignition (LOI) is not significant and never exceeds 1.9 wt.%.

The homogeneous dunite ($n = 4$), the layered dunite ($n = 3$) and the porphyritic dunite ($n = 3$) are broadly similar in terms of their major element compositions (given in wt.% below) by having a tight range of SiO_2 (40.3–42.4 wt.%), MgO (45.6–50.7 wt.%), FeO^t (6.52–8.00 wt.%), CaO (0.2 –0.8 wt.%), TiO_2 (0.01–0.05 wt.%) and mg# (91.0–93.3). However, the layered dunite has elevated Cr_2O_3 (1.40–2.80 wt.%) and Al_2O_3 (1.81–2.09 wt.%) relative to the two other units (0.26–0.58 wt.% and 0.24–1.22 wt.%, respectively), which is consistent with the larger modal chromite contents of the layered dunite.

The peridotite ($n = 5$) is significantly more variable in its major element composition than the above-mentioned dunite and has the following ranges: 34.6–47.1 wt.% SiO_2, 41.3–46.3 wt.% MgO, 7.76–11.6 wt.% FeO^t, 0.01–1.98 wt.% CaO, 0.04–0.08 wt.% TiO_2 and bulk-rock mg# of 87.0–90.8. Cr_2O_3 (0.93–5.69 wt.%) and Al_2O_3 (1.60–3.63 wt.%) is also significantly more variable for the peridotites, consistent with an even greater abundance of chromite than for the layered dunite. NiO correlates with MgO for all of the dunites and peridotite, and ranges from 0.25 wt.% to 0.50 wt.%.

The poikilitic peridotite ($n = 1$) is less magnesian (MgO of 39.2 wt.% and mg# of 89.3) than the above-mentioned peridotite, and more silica-rich (SiO_2 of 49.1 wt.%). This is consistent with the abundant orthopyroxene in this poikilitic peridotite. It has lower NiO (0.17 wt.%) and a relatively low Cr_2O_3 (0.68 wt.%) compared to the other rock types. The Seqi dunites and peridotites have a CaO/Al_2O_3 ratio less than 0.9 and Al_2O_3/TiO_2 ratios ranging from 25.4 to 70.3, which is comparable to those of the Fiskefjord peridotites reported by Szilas et al. (2015b).

The amphibolite ($n = 1$) is an outlier among the measured samples in that it has far higher TiO_2 (0.60 wt.%) and CaO (8.90 wt.%), in combination with low MgO (27.5 wt.%) and NiO (0.10 wt.%). The mg# of the amphibolite is 83.3, whereas the remaining major elements are in the same range as the other rock types from the Seqi Ultramafic Complex (Fig. 7).

Major element compositions of the chromitite samples ($n = 3$) are not plotted together with the other lithological units in Fig. 7, because of their extreme compositions caused by their high oxide contents. However, their SiO_2 contents is up to 20.1 wt.%, consistent with the presence of interstitial orthopyroxene (Figs. 4 and 5). Otherwise these rocks are dominated by the main components constituting chromite e.g., Cr, Al, Mg, Fe and minor Ti.

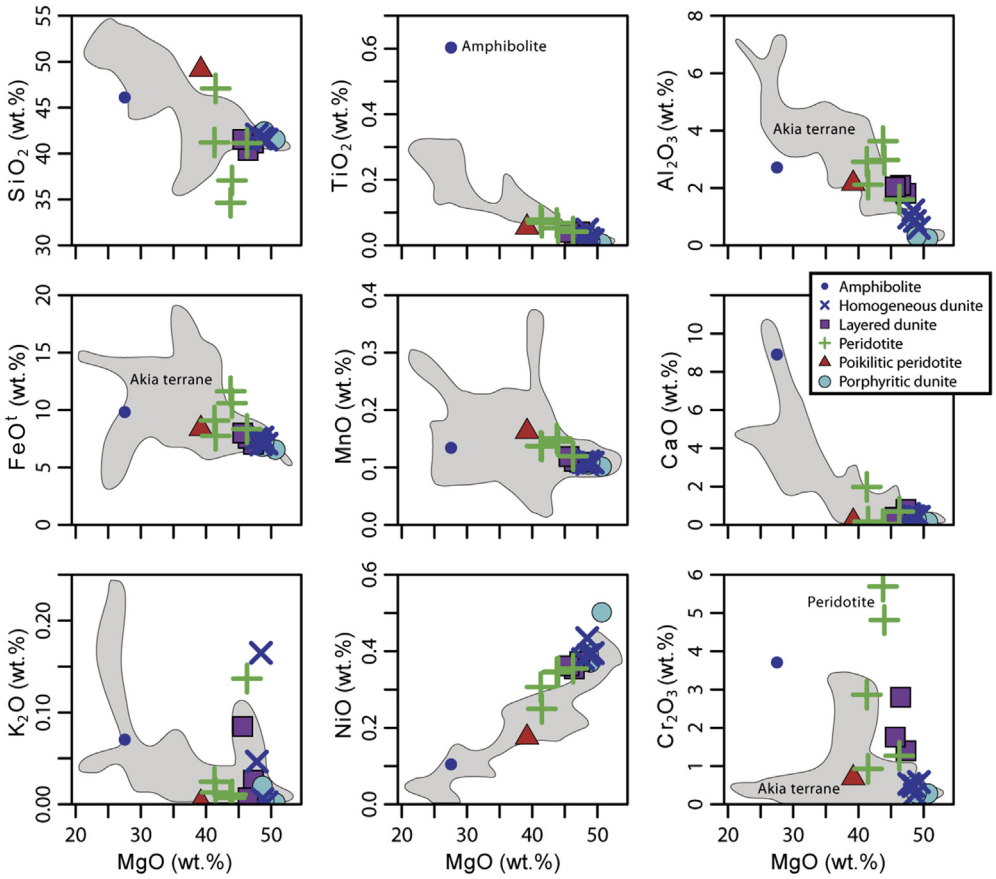

Figure 7. Bulk-rock major element compositions of the Seqi rocks (this study) plotted in comparison with regional data for regional ultramafic (MgO >20 wt.%) enclaves in the Mesoarchaean Akia terrane marked in grey shade (Akia data from: Garde, 1997; Kristensen, 2006; Szilas et al., 2015b). A similar comparison for trace elements is presented in Appendix D (Fig. D1). All of the new bulk-rock data for the Seqi rocks are available in the supplementary Table S1.

Normative mineralogy of the Seqi rocks was calculated using a modified CIPW-norm (Kelemen et al., 1992), which overall agrees with the observed modal mineralogy. The following normative chromite contents was calculated: the homogeneous dunite should have between 0.3 and 0.6 mol% chromite, the porphyritic dunite between 0.3 and 0.5 mol%, the poikilitic peridotite 0.8 mol%, the layered dunite between 1.4 and 2.8 mol%, the peridotite between 1.0 and 5.4 mol% normative chromite. The normative olivine content is calculated as: 93–96 mol% for the homogeneous dunite, 93–98 mol% for the porphyritic dunite, 49 mol% for the poikilitic peridotite, 88–93 mol% for the layered dunite, 60–93 mol% for the peridotite. The residual normative mineralogy is dominated by orthopyroxene, which is usually only predicted a few mol% for most of the Seqi rocks. Two exceptions are the poikilitic peridotite, which has 47 mol% normative orthopyroxene and one peridotite (186464) has 35 mol% normative orthopyroxene. These features are overall consistent with what is actually observed petrographically; however, the normative calculations are not able to determine the exact proportions of the minor Ca-bearing minerals that are present in the Seqi rocks units. The normative calculations suggest that plagioclase, rather than amphibole (or clinopyroxene) should be present, despite the fact that plagioclase is not observed in the modal mineralogy of any of the studied Seqi rocks.

Incompatible trace element compositions of the different rock types in the Seqi Ultramafic Complex appear to be controlled mainly by their modal chromite and amphibole contents (Fig. 8), which generally yields low and high abundances, respectively. There are a few exceptions in that Ti is elevated for the chromite-rich samples in addition to Pb, which is consistent with the *in situ* trace element data that we present in Section 5.4. Because the amphibolite sample is distinct from the rest of the Seqi samples and likely represents a metasomatic rock related to the intrusion of granitoid sheets, we disregard this single sample in the following consideration of the bulk-rock data and refer the reader to Appendix D for more information on this particular sample (Figs. D3 and D4 in Appendix D). Additional geochemical plots for the rest of the samples are also presented in Appendix D, and are referred to with the prefix 'D' in the discussion.

Regardless of their specific mineralogy the primitive mantle (PM)-normalised trace element patterns of the Seqi rocks share several common features. They have overall U-shaped patterns with elevated Th and U at up to 4 times PM values. They consistently have positive Pb–Zr–Hf anomalies and mostly negative Sr–Eu-anomalies and a fairly constant $(Nb/La)_{PM}$ with a median value of 0.6. All of the Seqi rocks also have U-shaped chondrite-normalised REE patterns with $(Gd/Yb)_N$ around 0.5 in combination with LREE enrichment (Fig. D2 in Appendix D), and generally negative Eu-anomalies.

5.2. Bulk-rock platinum-group element data

Platinum-group element (PGE) and Au data were determined for all of the different rock units. The homogeneous dunite ($n = 3$) and the porphyritic dunite ($n = 3$) have similar PM-normalised PGE patterns with the exception of one sample (186489), which has significantly lower Os and Ir abundances (Fig. 9). The PM-normalised

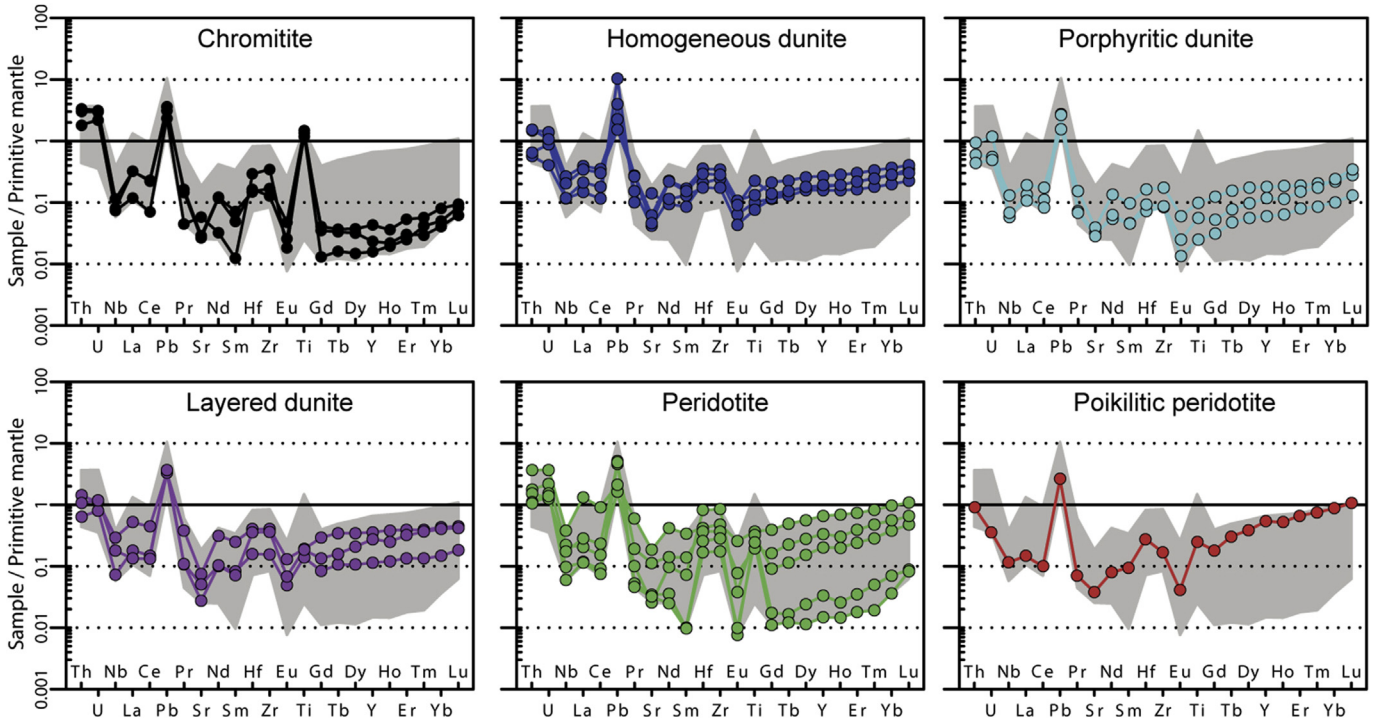

Figure 8. Bulk-rock trace element diagrams for the Seqi rocks normalised to primitive mantle (Palme and O'Neill, 2003). The shaded area outlines the total range of the data for comparison. Note the consistent positive Pb–Hf–Zr anomalies and the elevated Th–U–La relative to Nb, which may indicate some degree of contamination with continental crust. The negative Sr–Eu anomalies suggest fractionation in equilibrium with plagioclase from the parental magma, whereas the positive Ti reflects the addition of cumulus chromite. All of the new bulk-rock data for the Seqi rocks are available in the supplementary Table S1.

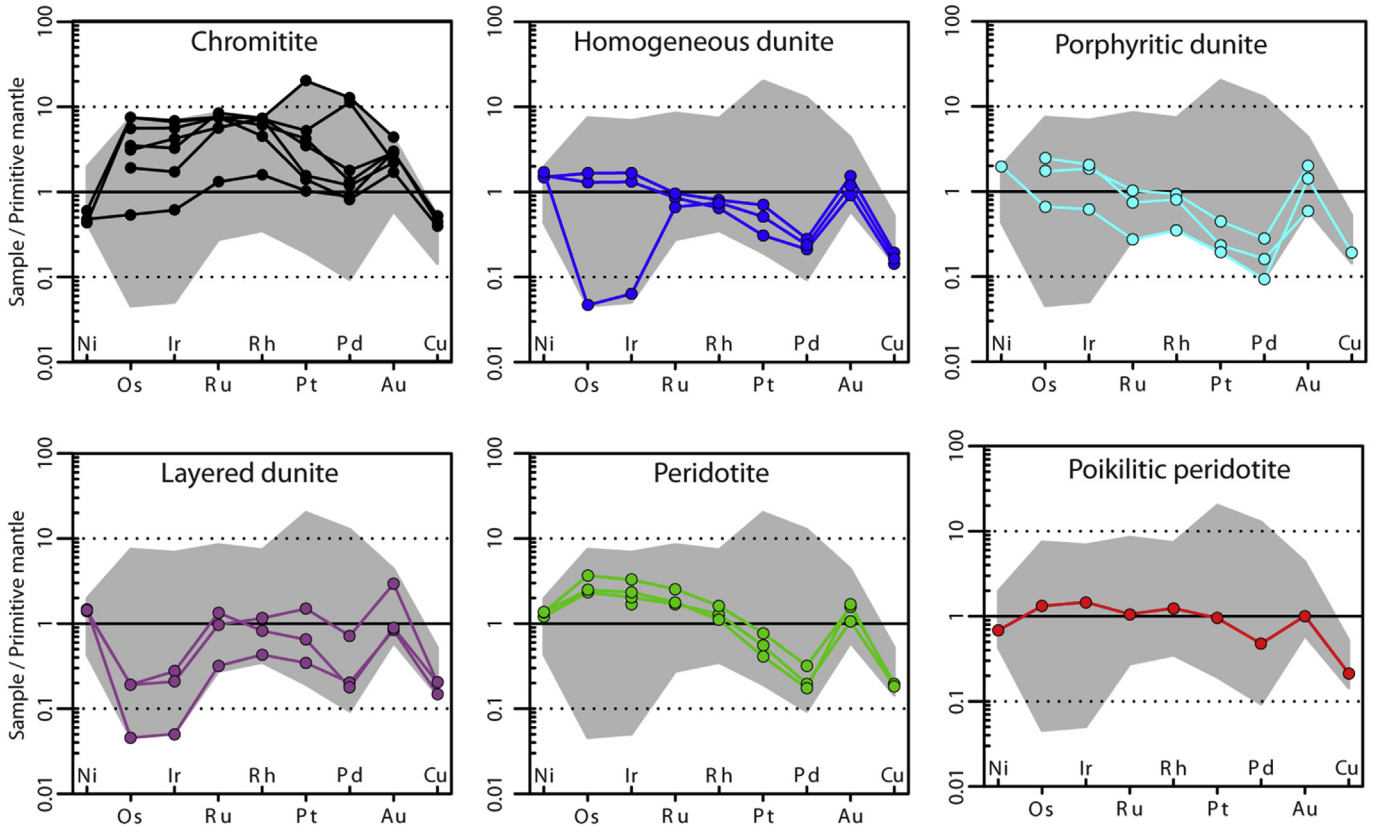

Figure 9. Bulk-rock siderophile element diagrams for the Seqi rocks normalised to primitive mantle (PM) of Becker et al. (2006). Note that most of the Seqi samples have elevated Os and Ir abundances relative to primitive mantle, and that their normalised patterns are generally negative with a distinct positive Au-anomaly. Four samples have troughs at Os and Ir, indicating early saturation of IPGE-alloys in these particular samples. There is a general positive correlation between IPGE abundances and chromite contents for the Seqi Ultramafic Complex (see Appendix D). The bulk-rock siderophile element data are available in the supplementary Table S2.

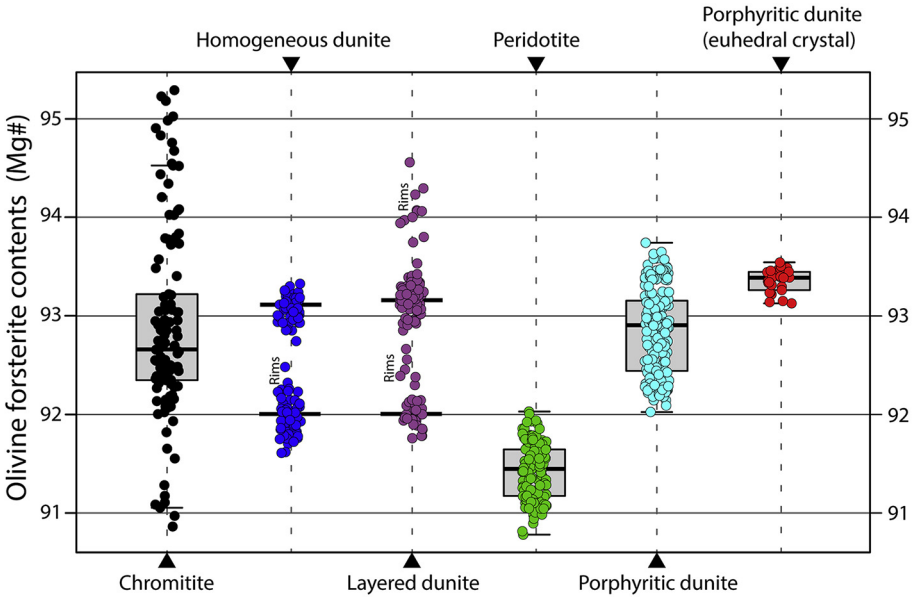

Figure 10. Olivine forsterite contents (Mg#) of the different rock units of the Seqi Ultramafic Complex (electron microprobe data). The median (thick lines) lies in a box that comprises 50% of the data (inter-quartile range; IQR) and the 'whiskers' extend to 1.5 times IQR on either side. Note that the layered dunite and the homogeneous dunite display a bimodal distribution, which is correlated with the bulk-rock mg# contents of these particular samples (see Fig. 11a). Note that these two rock types also show some scatter to higher forsterite compositions at rims in contact with spinel. Also note that in this work we distinguish between bulk-rock 'mg#' (which uses ΣFe) and mineral 'Mg#' (which uses Fe^{2+}). All of the electron microprobe data for the Seqi Ultramafic Complex are available in the supplementary Table S3.

PGE patterns generally have smooth negative slopes with distinct peaks for Au. The layered dunite samples ($n = 3$) all have a distinct trough at Os and Ir, but are otherwise mostly within the range of abundances as the other types of dunite. The poikilitic peridotite ($n = 1$) has flat PM-normalised pattern and PGE abundances similar to that of PM, although it also has a small positive Au-anomaly, caused by lower Pd and Cu abundances than for PM. The peridotite samples ($n = 3$) have similar PGE patterns as the homogeneous and porphyritic dunites, including the positive Au-anomalies. The chromitite ($n = 7$) is the most PGE-rich rock types at the Seqi Ultramafic Complex with ranges (in ppb) of Os from 2.12 to 29.3, Ir from 2.14 to 24.2, Ru from 9.31 to 60.3, Rh from 1.59 to 7.4, Pt from 7.96 to 156.3, and Pd from 5.90 to 92.5. Interestingly, the metasomatic amphibolite sample (186463) has even higher Os (45.7 ppb) and Ir (39.0 ppb) abundances than the chromitites (Fig. D5 in Appendix D). The amphibolite has a total ΣPGE content of 178 ppb, whereas the highest ΣPGE for chromitite is 181 ppb. There is an apparent negative correlation for the Seqi rocks between their bulk-rock mg# and Ir (and Os) abundances (Fig. D7 in Appendix D), which suggests that olivine was not the primary host of the PGEs.

5.3. Electron microprobe mineral data

Olivine is highly forsteritic (olivine Mg# given as molar Mg/[Mg + Fe^{2+}] × 100) in all of the Seqi rock units with the following compositional Mg# ranges: 90.9–95.3 for chromitite, 91.6–93.3 for homogeneous dunite, 91.8–94.6 for layered dunite, 90.8–92.0 for peridotite, 92.0–93.7 for porphyritic dunite and 93.1–93.5 for euhedral crystals in the porphyritic dunite (Fig. 10). Olivine is essentially unzoned in all the Seqi rocks and only displays slight enrichment in Mg# at the rims where grains are in contact with chromite (Fig. D19 in Appendix D). This disturbance of Mg# is particularly pronounced for the chromitites (Fig. 10), where olivine grains extend to the highest Mg# recorded among all of the Seqi rock types, which is consistent with subsolidus Fe–Mg exchange between spinel and olivine.

As seen in Fig. 10, the olivine compositions of the layered dunite and the homogeneous dunite have an apparent bimodal forsterite distribution (Mg# of around 92.0 vs. 93.2). However, this feature is generally uncorrelated with the bulk-rock mg# of the measured samples, which is mainly determined by the modal spinel contents of the rocks (Fig. 11a). This effect is obvious for the peridotites, which have the lowest overall forsterite contents, and yet their bulk-rock mg# displays the largest range of the Seqi rocks, which suggests that olivine Mg# is independent of the chromite contents.

NiO in olivine does not show any systematic variation among the different lithological units, which have the following ranges: 0.33–0.61 wt.% for chromitite, 0.30–0.53 wt.% for homogeneous dunite, 0.35–0.51 wt.% for layered dunite, 0.33–0.56 wt.% for peridotite, 0.26 –0.58 wt.% for porphyritic dunite and the euhedral crystals in the porphyritic dunite have a range of 0.32–0.51 wt.%. The median NiO contents of the Seqi olivine is 0.44 wt.% (Fig. D8 in Appendix D).

Oxides in the different rock units of the Seqi Ultramafic Complex are generally Cr-rich spinel, hereafter simply referred to as chromite or spinel interchangeably. The spinel data were filtered by excluding analyses with significant Si + Na (>0.006 cpfu), given that these two elements are incompatible in the spinel structure and therefore likely reflect inclusion-rich grains. Chromite with >0.5 cpfu Fe (and Fe^{3+}# > 15) is assumed to represent grains that were affected by metamorphic re-equilibration, which is supported by their general enrichment in Mn and Ti, in combination with low Mg content (Fig. D13 in Appendix D). These characteristics are typical of metamorphosed chromite and can be used to discriminate such grains from primary igneous spinel compositions (Hattori and Guillot, 2007; Bernstein et al., 2013; Colás et al., 2014). Spinel in the Seqi rocks is generally unzoned, but do display elevated Cr# and low Mg# at rims in contact with olivine. This is also the case when spinel is being replaced by chlorite. There is clear evidence of secondary processes affecting the chromite rims to yield Cr-rich magnetite, which is also associated with an increase in TiO_2 by residual enrichment (Fig. D13 in Appendix D). An example of this reaction is seen in Fig. 5, where the 'spongy' texture of the spinel in the homogeneous dunite, is caused by replacement of chromite with chlorite, resulting in Fe–Ti–Mn-enrichment in the residual

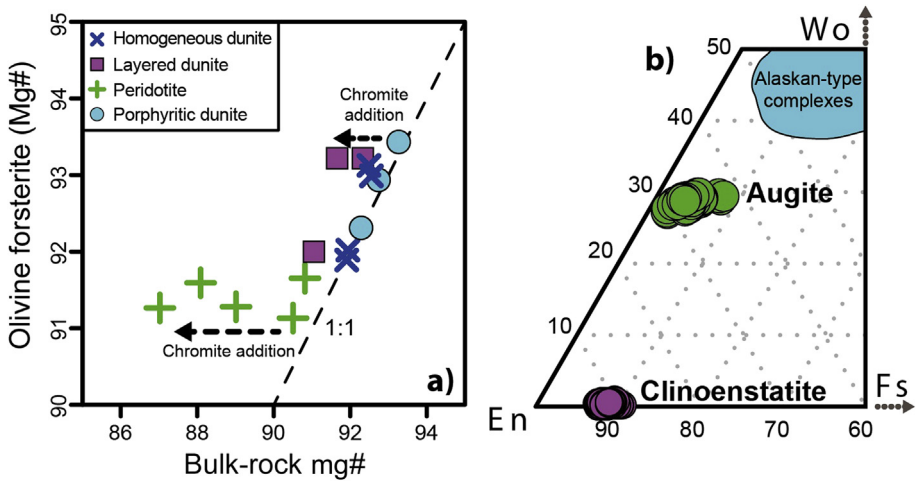

Figure 11. (a) Forsterite contents versus bulk-rock mg# for the Seqi rocks, showing a consistent olivine composition regardless of the bulk-rock composition (horizontal trends). This suggests that the olivine compositions reflect the primary Mg/Fe ratio of the melt at the time it crystallized, and that the bulk-rock compositions are the result of accumulation of Fe-rich cumulus chromite. (b) Part of the pyroxene ternary diagram with the endmembers of wollastonite (Wo), enstatite (En) and ferrosilite (Fs), showing the composition of the measured Seqi amphibole converted to corresponding anhydrous clinopyroxene compositions, as well as the measured orthopyroxene compositions. Note that if the inferred augite composition is representative of the igneous conditions, it would point to temperatures of above 1300 °C according to the experimental work of Lindsley (1983) and Lindsley and Andersen (1983). NB. Clinopyroxene has not been directly observed in any of the studied rocks from the Seqi Ultramafic Complex, although we expect this mineral to have been a primary igneous phase (see Section 5.3).

chromite to the point that it becomes Fe-rich chromite with essentially no Mg or Al, which are taken up by the newly formed chlorite.

The spinel Cr# (calculated as molar Cr/[Cr + Al] × 100) ranges from 26.4 to 97.4 for the various types of dunite and peridotite, but forms a much tighter range from 55.7 to 70.1 for the chromitite. The same is observed for spinel Mg#, which ranges from 15.4 to 62.9 for the dunite and peridotite and from 33.7 to 50.5 for the chromitite (Fig. 12). Spinel Fe^{3+}# is calculated assuming stoichiometry (given by molar $Fe^{3+}/(Fe^{3+} + Al + Cr) \times 100$) and generally falls below about 20, with the exception of the anomalous amphibolite sample (186463), which plots at just over 40. This sample also contains abundant ilmenite (Fig. D9 in Appendix D).

All of the pyroxenes that were measured are nearly pure enstatite orthopyroxene, regardless of their lithological host and form a tight range of compositions from $En_{89.4}$ to $En_{92.4}$, $Fs_{7.19}$ to $Fs_{10.4}$, and $Wo_{0.07}$ to $Wo_{0.09}$ (Fig. 11b). TiO_2 is less than 1.1 wt.%, Al_2O_3 is less than 2.6 wt.% and the median Cr_2O_3 contents is 0.21 wt.%. Their Mg# ranges from 89.4 to 92.6 (median of 91.0).

Amphibole is present mainly in the peridotite and the amphibolite units of the Seqi Ultramafic Complex, although minor amounts are also found in some of the different types of dunites. Two types of amphibole are found: (1) tremolite is mainly present in the amphibolite unit and as inclusions within euhedral olivine crystals of the porphyritic dunite, (2) magnesio-hornblende is present in the peridotite, as well as a minor phase in the various dunites. The attribution scheme of Hawthorne et al. (2012) was used to calculate the amphibole compositions and to estimate the Fe^{3+}/Fe^{2+} ratio.

Tremolite Mg# (in the C-site) ranges from 96.2 to 100. SiO_2 ranges from 47.1 to 55.7 wt.% (Si of 7.24 to 7.99 cpfu). TiO_2 is less than 0.8 wt.% (Ti < 0.07 cpfu), Cr_2O_3 is less than 1.8 wt.% (Cr < 0.13 cpfu), Fe^{3+} is less than 0.25 cpfu, Fe^{2+} is less than 0.19 cpfu, while MgO is up to 23.5 wt.% (Mg < 4.85 cpfu at the C-site). Magnesio-hornblende Mg# (in the C-site) ranges from 95.5 to 99.9. SiO_2 ranges from 48.6 to 58.2 wt.% (Si from 6.74 to 7.44 cpfu). TiO_2 is less than 0.7 wt.% (Ti < 0.09 cpfu), Cr_2O_3 is less than 1.4 wt.% (Cr < 0.20 cpfu), Fe^{3+} is less than 0.42 cpfu, Fe^{2+} is less than 0.21 cpfu, while MgO is up to 23.8 wt.% (Mg < 4.52 cpfu at the C-site).

Amphibole is interpreted to be metamorphic in origin, and to represent replacement of primary igneous pyroxene. In Fig. 11b, amphibole compositions have been recalculated on a volatile free basis and converted to the corresponding pyroxene stoichiometry. As can be seen in Fig. 11b, the corresponding pyroxene composition would range in from $En_{62.5}$ to $En_{70.5}$, $Fs_{2.08}$ to $Fs_{8.10}$, and $Wo_{27.0}$ to $Wo_{29.8}$, and would thus be clinopyroxene (augite). However, we note that if orthopyroxene has participated in the reaction of clinopyroxene to form metamorphic amphibole, it would not allow for the clinopyroxene composition to be reconstructed per the above recalculation. A clinopyroxene precursor origin for amphibole is supported by the *in situ* LA-ICP-MS mineral data presented in the following section that show negative Ta–Nb–Ti-anomalies (Fig. 13). Further evidence for the presence of igneous clinopyroxene is the elevated Ti content in some spinel rims, which has been interpreted to represent metamorphic re-equilibration and redistribution of Ti. Clinopyroxene can contain significant Ti in ultramafic igneous rocks and is a potential source of this Ti enrichment in spinel. Given that Ti mobility in aqueous fluids is low, this argues against a metasomatic introduction. Residual enrichment of Ti (and Fe + Mn) in spinel has also been observed, but only where chlorite replaces spinel, which represents a much later retrogression (see above and Fig. 5 and Fig. D13 in Appendix D).

5.4. *In situ LA-ICP-MS mineral data*

The trace element contents of the main rock-forming minerals (olivine, chromite, orthopyroxene and amphibole) in the Seqi Ultramafic Complex were measured *in situ* by LA-ICP-MS. Olivine has low levels of incompatible trace elements with the exception of large positive anomalies for Pb at up to 3 times primitive mantle abundances (Fig. 13). Chromium, Al, V and, to a lesser extent, Zn concentrations are affected by small spinel inclusions in the olivine, and the true concentrations in olivine appear to be a factor of 10 lower for Al, Cr and V, and a factor of 2 lower for Zn.

Spinel is the second-most depleted mineral. Besides enrichment in Pb, chromite has large positive anomalies for Ti. Orthopyroxene has a relatively smooth U-shaped trace element pattern with distinct positive anomalies for Th–U–Pb–Ti. Amphibole is the

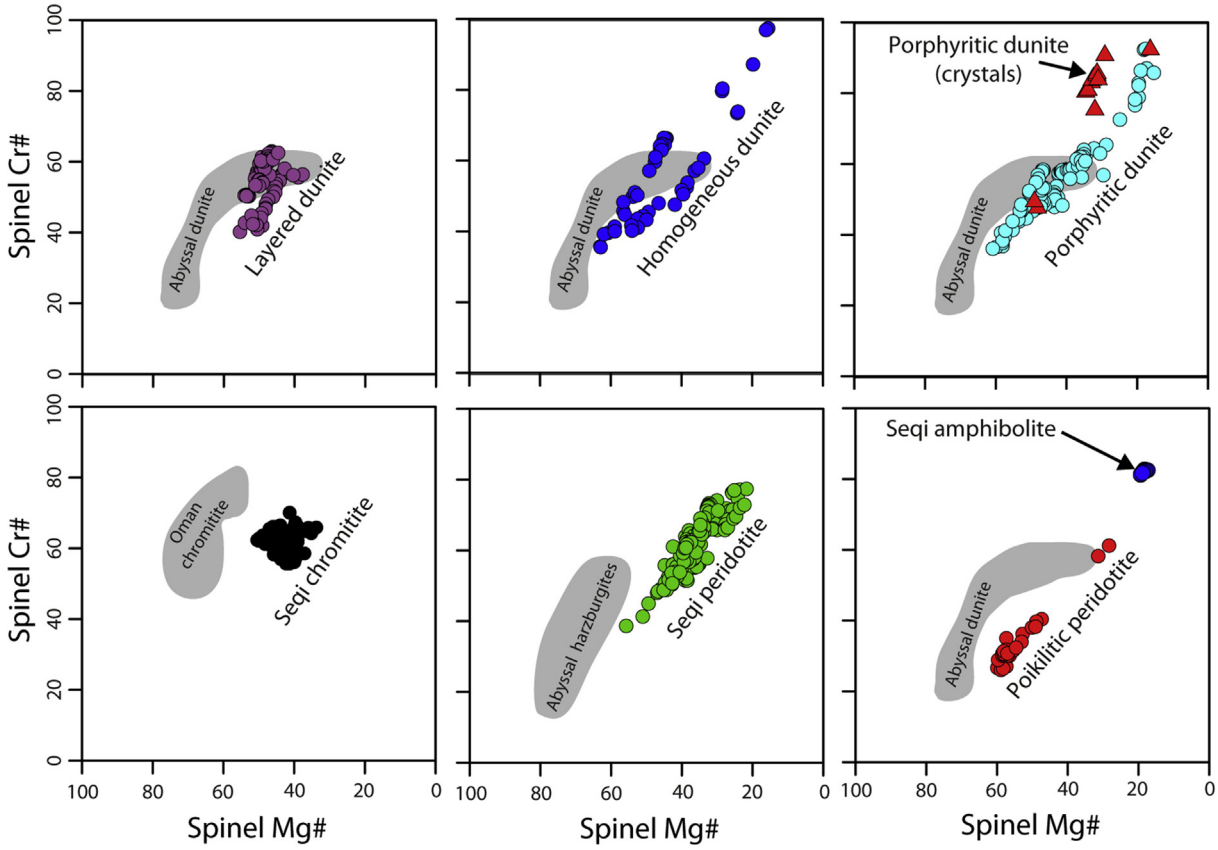

Figure 12. Spinel compositions from the Seqi Ultramafic Complex. The fields of abyssal harzburgite (residual mantle) and dunite (melt channels) are from Warren (2016) and the field of Oman chromitite is from Rollinson (2005). The spinel compositions clearly demonstrate that the Seqi Ultramafic Complex does not represent a mantle fragment. The electron microprobe mineral data for the Seqi Ultramafic Complex are available in the supplementary Table S3.

most incompatible trace element-rich mineral, and generally has negative anomalies for the high field strength elements (HFSEs). Phlogopite is enriched in large ion lithophile elements (LILEs) in addition to Nb–Ta–Ti, but this mineral is not present in modal abundances that would make it critical in bulk-rock reconstruction of any of the rock types at the Seqi Ultramafic Complex. Futhermore, it likely represents a metasomatic product related to the fluid infiltration from the intruding granitoid host rocks.

5.5. Zircon U–Pb isotope ages

Sample 186456 (tonalitic orthogneiss) has zircon grains that are mainly prismatic with aspect ratios around 2 to 4 and lengths of 200–300 μm. Zircon grains contain a variety of internal textural domains, with both growth zoned or homogeneous cores and inclusion rich rim domains. Fig. 6a shows examples of the different domains, where preserved growth zoning is observed in grains a1 and a2. In grain a3 the core domain appears homogeneous and one end of the grain is strongly disturbed and inclusion rich. In grains a4 and a5 disturbed domains are observed as back-scattered electron (BSE) dark regions, however remaining original zoning patterns are also observed. Zircon U–Pb isotope analyses have mainly been focused on core domains, with few spots placed in rim domains in this sample. The disturbed rim domains are relatively rich in common-Pb and analyses with low $^{206}Pb/^{204}Pb$ have been corrected for common-Pb. The data are mainly concordant and except for four analyses the remaining 39 spots are within ±10% of discordance. Th/U values mainly range from 0.1 to 0.5 with the lowest values corresponding to some of the lowest ages, however they do not display any obvious trends. $^{207}Pb/^{206}Pb$ ages range from 2749 to 2997 Ma and by choosing analyses in core domains with least textural evidence for disturbance, an average $^{207}Pb/^{206}Pb$ age of 2977 ± 7 Ma ($n = 15$; MSWD = 0.67) is obtained for this sample. Using the same data an intercept age of 2978 ± 8 Ma is obtained (Fig. 14a), and this age is interpreted to represent the intrusive age of the orthogneiss protolith.

Sample 186451 (tonalite sheet) has zircon grains that are large (mainly > 300 μm) and stubby with aspect ratios from 1 to 3. Internal textures are mainly homogeneous, many grains have rather wide zones that are parallel to the crystal faces (Fig. 6b). Some grains have narrow rims or partial rims with irregular boundaries toward the core of the grains and low BSE intensity (Fig. 6b, grains b2, b3). Trails of inclusions are present in many grains and they commonly occur in two to three orientations (Fig. 6b, b1, b3). Zircon grains from this sample are relatively poor in U (mean of 50 ppm) and the ^{204}Pb signal is mainly at background levels. Analyses are concordant and plot in a rather narrow group (Fig. 14b). The average of all analyses (rejecting outliers on a 2σ level) yield an age of 2969 ± 5 Ma ($n = 41/45$; MSWD = 0.92). This age is interpreted to reflect the crystallisation age of the tonalitic sheet, which is indistinguishable from sample 186456 within the error of the analyses.

Sample 186453 (pegmatite) has zircon grains that are prismatic. The grains have a large variation in sizes from 100 to 700 μm, with the larger grains being more abundant. These grains have a brownish colour. Internal textures are divided into two main domains; internal core regions, which are mostly either homogeneous or growth zoned and BSE bright regions which are, often rims domains (Fig. 6c). The BSE bright domains are commonly inclusion

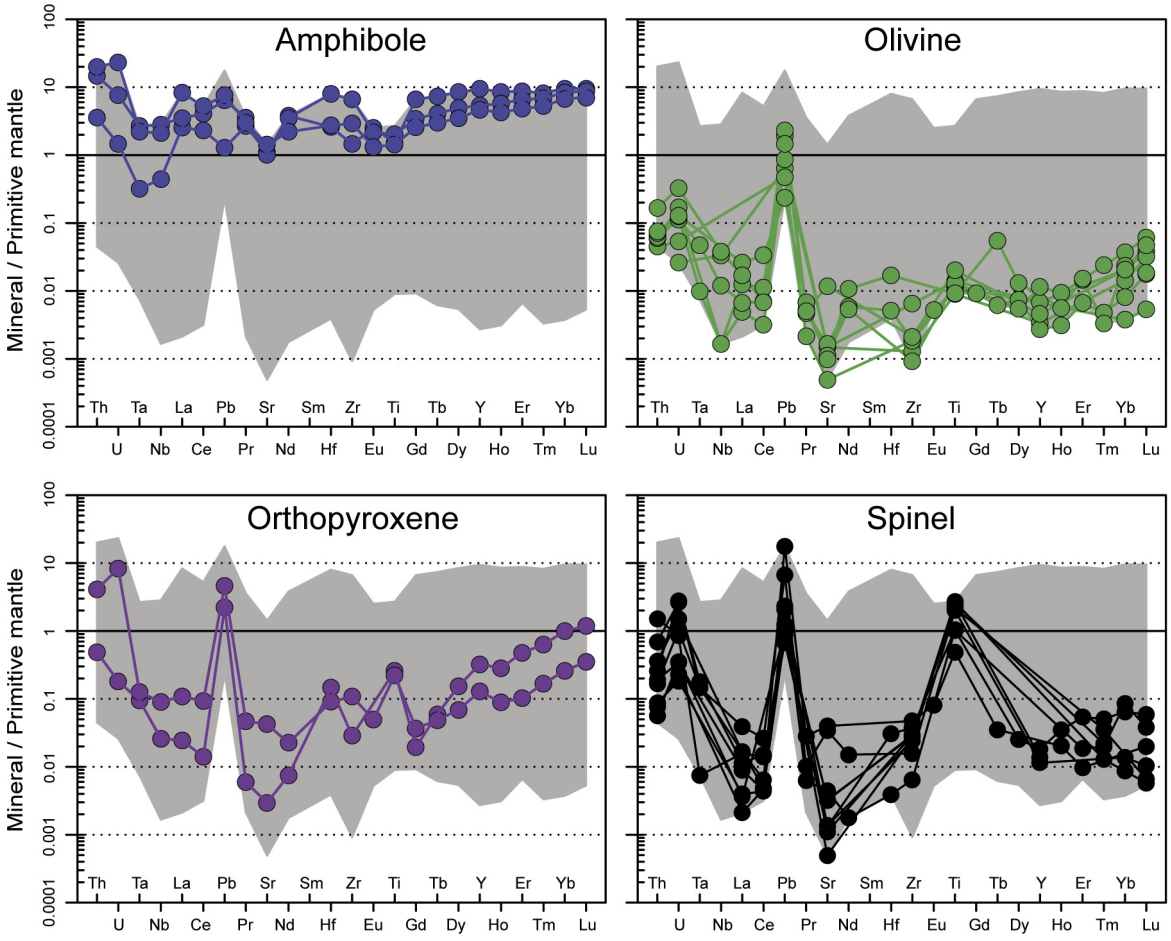

Figure 13. LA-ICP-MS trace element data for individual minerals from the Seqi Ultramafic Complex normalised to primitive mantle of Palme and O'Neill (2003). Note that amphibole has the highest abundance of incompatible trace elements of the measured minerals, and that it displays negative anomalies for Ta-Nb-Ti, which may indicate it originally formed as igneous clinopyroxene, rather than representing igneous amphibole. Also, note that spinel is enriched in Ti (and Ta), and thus could impose negative anomalies for these particular elements on the magma from which it crystallized, which is indeed observed in tholeiitic metabasalts of this region (e.g., Garde, 2007; Polat et al., 2011; Szilas et al., 2014b). The grey area marks the total range of the Seqi mineral data. The LA-ICP-MS data for the Seqi Ultramafic Complex are available in the supplementary Table S4.

rich (Fig. 6c, grain c2) and contain irregular low intensity BSE regions (Fig. 6c, c1). Zircon U–Pb isotope analyses have mainly been focused on core domains. There is a high common Pb contents in many of the analyses, and overall a positive correlation between $^{206}Pb/^{204}Pb$ and $^{207}Pb/^{206}Pb$ age is observed. Common-Pb is mainly present in BSE bright rim domains, buts also in some texturally undisturbed core regions. Analyses are generally concordant, and plot in one coherent group (Fig. 14c), which range in age from 3014 to 2816 Ma. There is no observable correlation between Th/U and $^{207}Pb/^{206}Pb$ age. By selecting analyses from unaltered core domains an average $^{207}Pb/^{206}Pb$ age of 2940 ± 5 Ma (n = 59/65; MSWD = 1.4) is obtained, which is interpreted as the crystallisation age of the pegmatite. Analyses from BSE bright rim domains yield a $^{207}Pb/^{206}Pb$ age 2915 ± 10 Ma (n = 20/21; MSWD = 1.2), which suggest that Pb-loss affected these regions; however, this age might not have any geological meaning.

5.6. Mössbauer spectroscopy data

Mineral separates from five chromitite samples were analysed by the Mössbauer method at Derby University using the procedure described by Rollinson et al. (2012). The following $Fe^{3+}/\Sigma Fe$ ratios were determined: 0.157, 0.184, 0.192, 0.209 and 0.470. In Fig. 15, we present two of the obtained spectra as examples of models (1) and (3), respectively (see Section 4.6). The remaining spectra, as well as the data, are given within Table S6. A single sample (186469) has elevated $Fe^{3+}/\Sigma Fe$ of 0.470, and it also has relatively low PGE contents (Section 5.2) and low SiO_2 (4.50 wt.%), but is otherwise similar to the rest of the chromitite samples. However, this sample has the largest range in spinel Fe^{3+}# from 8 to 15, elevated spinel Mg# of about 50, and it is the most chlorite-rich of the chromitite samples. Therefore, it appears that this particular sample was affected by metamorphic retrogression, which resulted in formation of Cr-rich magnetite, as well as chlorite at the expense of igneous chromite (Fig. 5). All the results of the $Fe^{3+}/\Sigma Fe$ obtained from Mössbauer analyses are plotted in Fig. 16, along with estimates based on EMPA and LA-ICP-MS measurements of spinel calculated by assuming stoichiometry.

5.7. P–T constraints and metamorphic history

The igneous paragenesis of the Seqi Ultramafic Complex is dominated by olivine, chromite, orthopyroxene, and variable clinopyroxene (which is now present as amphibole, see Section 6.2). There is no petrographical, nor geochemical evidence for garnet having been present in these rocks, which constrains the upper pressure of emplacement to ~2.4 GPa, below which spinel is the aluminous phase. The olivine–spinel Al-exchange thermometer of

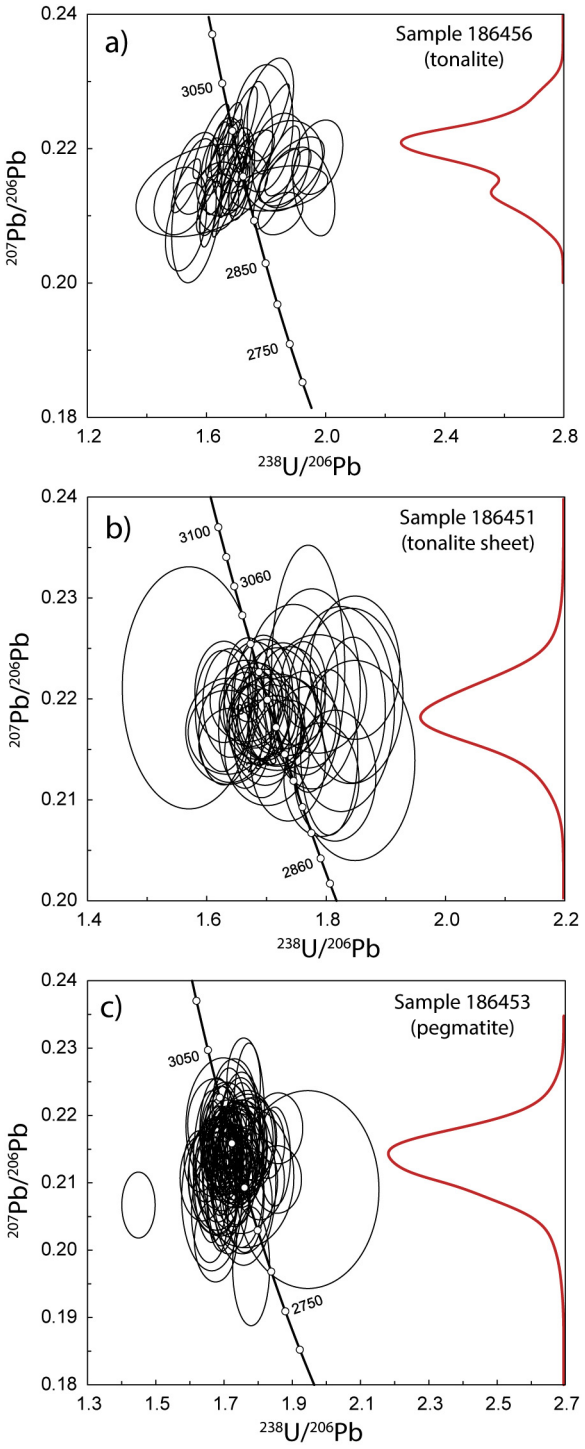

Figure 14. Tera-Wasserburg concordia diagrams for the three intrusive granitoid rocks at the Seqi Ultramafic Complex. The red curve at the right side of each diagram displays the cumulative distribution of the $^{207}Pb/^{206}Pb$ ratios and the error ellipses represent 2σ error. (a) Sample 186456 (tonalitic orthogneiss) has an interpreted magmatic age of 2978 ± 8 Ma. (b) Sample 186451 (tonalite sheet) has an interpreted magmatic age of 2963 ± 6 Ma. (c) Sample 186453 (pegmatite) has an interpreted magmatic age of 2940 ± 5 Ma. All of the U-Pb isotope data for the three granitoid rocks are available in the supplementary Table S5.

Wan et al. (2008), when applied to spinel core compositions and the 3rd quartile Al content of associated olivine cores, provides temperature estimates between 1200 and 1250 °C. Olivine–spinel rims in direct contact give Al-temperatures that are 50 °C lower, indicating some, but minor, re-equilibration of Al-contents during subsequent metamorphism. The 1200–1250 °C temperature is close to the dry peridotite solidus and indicates that the parental melt had an activity of H_2O of <0.15 at high pressure or essentially dry at the low end of the pressure range.

Preservation of magmatic structures and textures in chromite and olivine on outcrop and thin section scales indicates limited metamorphic mineral replacement despite granoblastic textures, and minimal hydration, in agreement with overall dry conditions. Minor tremolite inclusions suggest initial cooling to below ~680 °C, but the peak metamorphic stage does not contain amphibole, except in samples that we interpret as not preserving their magmatic compositions. Peak metamorphic assemblages for the various Seqi rocks are olivine + spinel, olivine + spinel + orthopyroxene, and olivine + spinel + orthopyroxene + phlogopite. Clinopyroxene would also have been stable at this stage if its presence is accepted.

P–T conditions for this peak metamorphic stage were constrained by constructing pseudosections using PerpleX (Connolly, 2005), using the thermodynamic database of the Holland and Powell (2011) and associated solution models for amphibole, olivine, pyroxene, Cr-spinel, serpentine, talc, garnet, biotite and plagioclase (Diener and Powell, 2012; Jennings and Holland, 2015). The presence of phlogopite as the sole K-bearing and hydrous phase in sample 186489 limits the water content to between 0.05 and 0.15 wt.%, and a common value of 0.1 wt.% was used in all calculations. Also note that Cr was included in the pseudosection calculations to account for the effect that it has on increasing the spinel stability range. Fig. 17 shows the fields where the sample paragenesis is predicted to be stable for each sample. These fields overlap to constrain conditions from 700 to 900 °C at 1.0 to 2.3 GPa, bordered by the lack of garnet (maximum *P*), clinopyroxene (maximum *T*), plagioclase (minimum *P*) and various hydrous phases (minimum *T*). If clinopyroxene was present at this stage, the pressures and temperatures could potentially have been higher (dashed field in Fig. 16).

A variety of geothermometers was applied to mineral rim compositions and contact mineral pairs (Fig. 17 inset). Mg–Fe exchange thermometers underestimate temperatures, likely owing to low blocking temperatures for Mg–Fe inter-diffusion, whereas olivine–orthopyroxene Ni-exchange may suffer from incomplete metamorphic equilibration. Ca-solubility thermometry should strictly be regarded as minimum temperature estimates, because the Ca-saturating phase clinopyroxene is missing, but we interpret this to be an absence related to retrogression consistent with regional interpretations (Garde, 1997). The geothermometers converge to the lower temperature half of the pseudosection field.

Peak metamorphism was followed by several retrogression episodes, producing varying amounts of amphibole, serpentine and talc, followed by chlorite, and leading to retrogression of chromite to Cr-magnetite and further to chlorite. This retrogression is accompanied by hydration, and may have been instigated by granitoid intrusion given the similarity in mineral phases in the granitoid-ultramafic reaction rims.

6. Discussion

A large ultramafic rock body like that of the Seqi Ultramafic Complex could either represent a mantle fragment or olivine-rich cumulates derived by fractional crystallisation processes in the crust. In the latter case one would need to distinguish between: (1) komatiite-related dunite formed by inflation of a lava flow channel (Arndt et al., 2008), (2) a layered intrusive complex formed by *in situ* crystal fractionation, as exemplified by world-class localities like the Bushveld, Muskox, Skaergaard and Stillwater complexes (Irvine, 1977; McBirney and Noyes, 1979; McCallum et al., 1980;

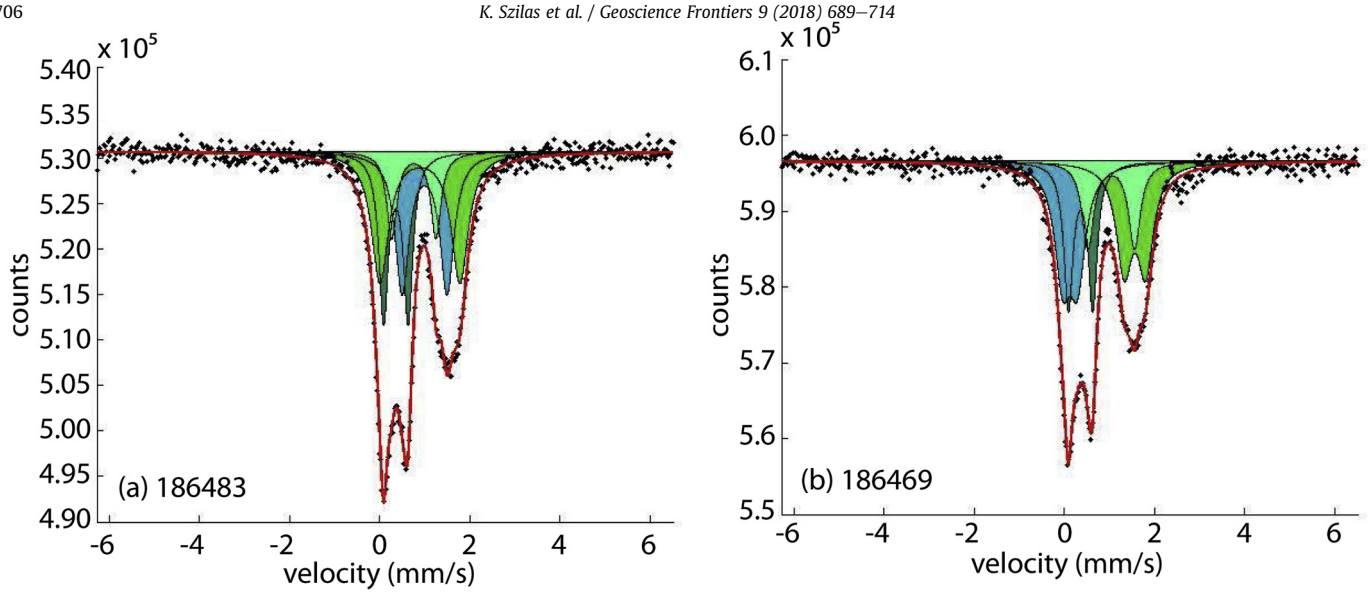

Figure 15. Examples of room temperature Mössbauer spectra of chromite in chromitite samples 186483 (a) and 186469 (b) from the Seqi Ultramafic Complex. The spectra were fitted as $3Fe^{2+}(A) + 1Fe^{3+}(B)$ and $Fe^{2+}(A) + Fe^{2+}(B) + Fe^{3+}(B)$, respectively. The data and the remaining spectra are provided in the supplementary Table S6.

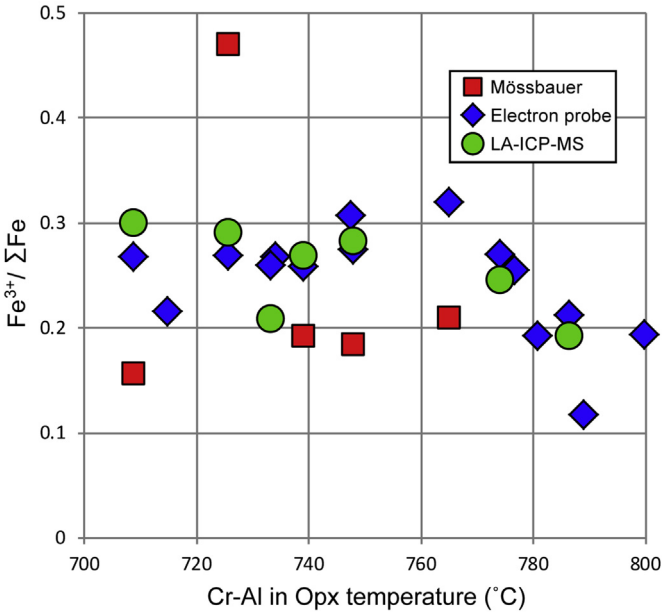

Figure 16. Constraints on the oxygen fugacity of the Seqi rocks given as $Fe^{3+}/\Sigma Fe$. The Fe^{3+} proportion was determined by Mössbauer spectroscopy in addition to measurements by electron microprobe and LA-ICP-MS assuming spinel stoichiometry (see Section 5.3). The data are plotted against temperatures calculated by Cr-Al in orthopyroxene in the same samples, and are thus only given for samples in which this mineral was present.

Eales and Cawthorn, 1996; Spandler et al., 2005; Nielsen et al., 2015), or (3) alternatively a zoned Ural-Alaskan type ultramafic complex, which represents arc-related magma conduits (Irvine, 1974; Burns, 1985; DeBari and Coleman, 1989). In the following discussion, these different hypotheses are evaluated by employing a holistic approach to the new bulk-rock and mineral geochemical data presented in the previous sections.

6.1. Bulk-rock geochemical features

Mantle rocks represented by dunite should either have formed as highly depleted residues that experienced large degrees of melt extraction or alternatively they could be the products of melt-rock interaction (e.g., Kelemen et al., 1992; Bernstein et al., 1998). Cumulate dunite formed in the crust on the other hand forms by olivine segregation from a magnesian magma, and it would be mineralogically similar, but petrographically distinct. However, the Seqi Ultramafic Complex has experienced granulite- to upper amphibolite-facies metamorphism, which is consistent with the persistent granoblastic textures (Figs. 4 and 5), and thus the petrographical features are difficult to directly apply to this distinction.

Both mantle rocks and peridotite cumulate rocks formed within the crust should theoretically have extremely low trace element abundances due to the loss of these components and lack of incorporation in fractionating olivine, respectively. It should be to noted that all of the Seqi peridotites (*s.l.*, including the dunites) have elevated Th contents, whereas abyssal, ophiolitic and orogenic peridotites commonly have negative Th-anomalies (Bodinier and Godard, 2003; Niu, 2004). Despite this obvious difference, the overall trace element abundances of the Seqi rocks are nonetheless similar to those of mantle rocks (Fig. D21 in Appendix D). Recently, however, it has become clear that the incompatible trace element contents of mantle residues are far more enriched than can be accounted for by melt extraction models (Warren, 2016). This means that trace element abundances are controlled to a higher degree by melt-rock reaction than by pure melt depletion, and thus trace element patterns are hardly a diagnostic feature of mantle rocks.

When comparing the major element compositions of abyssal peridotites with those of the Seqi rocks (Fig. D20 in Appendix D), it is noted that the latter extend to far higher MgO, Ni and Cr and have lower CaO and SiO_2 contents. The chromite compositions of the Seqi rocks also argue against them representing mantle rocks (Fig. 12), as will be discussed further in Section 6.2.

The Seqi bulk-rock compositions show better geochemical overlap with olivine-rich cumulates associated with komatiites (Fig. D27 in Appendix D). However, the Al_2O_3/TiO_2 ratios of the Seqi rocks are around 40, which is significantly different from that of the two main types of komatiite (Barberton-type ~ 15 and Munro-type ~ 19). The peridotites (MgO>20 wt.%) of the Fiskefjord region have an average value of around 42, which agrees with the Seqi rocks and clearly distinguishes them from komatiitic cumulates (Fig. 18). The CaO/Al_2O_3 ratios of the Seqi rocks are generally low (<0.44). The Al_2O_3 contents of the Seqi rocks is controlled by the modal contents of

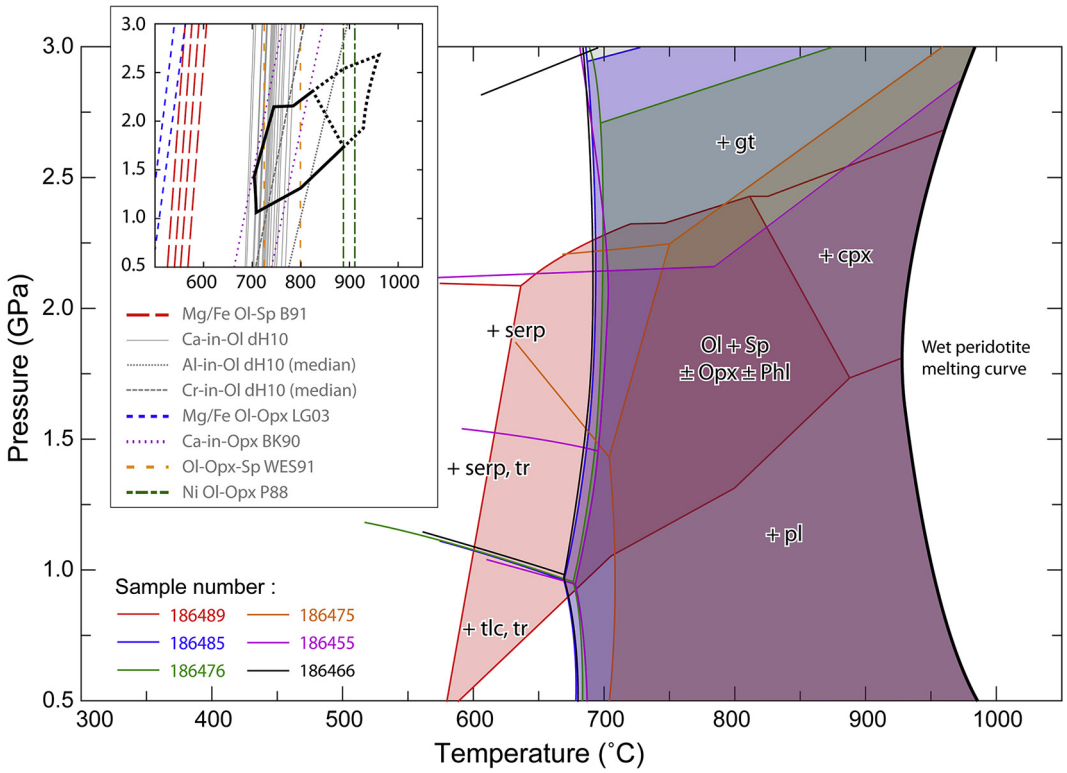

Figure 17. Pressure versus temperature phase diagram showing calculated pseudosections for six ultramafic rock from the Seqi Ultramafic Complex. Estimated pressure-temperature conditions for peak metamorphism of the Seqi Ultramafic Complex are 700 to 900 °C at 1.0–2.3 GPa, as constrained from the overlap in pseudosection mineral assemblage fields for six samples ranging from dunite, to peridotite, to chromitite, to amphibolite. This field is bounded by the lack of clinopyroxene, garnet, plagioclase, talc, tremolite and serpentine at peak conditions. If clinopyroxene was present, the field expands to higher pressure and temperature (dashed field in the inset). The inset shows additional constraints from geothermobarometers applied to mineral rims and contact pairs. P88-Ni–Mg exchange between olivine and orthopyroxene (Povdin, 1988); BK90-Ca in orthopyroxene (Brey and Köhler, 1990); B91-Mg–Fe exchange between olivine and spinel (Ballhaus et al., 1991); WES91-Al in orthopyroxene (Witt-Eickschen and Seck, 1991); LG03-Mg–Fe exchange between olivine and orthopyroxene (Liermann and Ganguly, 2003); dH10-Ca, Al and Cr in olivine (de Hoog et al., 2010). The following mineral abbreviations are used: amphibole (Am), clinopyroxene (Cpx), garnet (Grt), orthopyroxene (Opx), phlogopite (Phl), plagioclase (Plag), spinel (Spl), olivine (Ol), serpentine (Srp), talc (Tlc), and tremolite (Tr).

chromite, which is generally high in comparison to komatiitic cumulates, as also seen by the elevated Cr of the Seqi rocks (Fig. 18). Additionally, the moderately incompatible trace element abundances of the Seqi rocks (including TiO_2) are relatively low, giving them U-shaped patterns, which is evident from a significantly lower $(Gd/Yb)_N$ ratio than for komatiitic cumulates (Fig. 18).

The PGE patterns of the various Seqi dunites display either a relatively smooth negative pattern at around 1 to 0.1 times PM or an IPGE-depleted pattern (Fig. 9). None of these patterns resemble those of dunite channels in the Oman mantle section, which have scattered patterns due to local sulfide dissolution by percolating melts (Hanghøj et al., 2010). Strong negative IPGE (iridium-affinity PGEs) fractionation is a typical feature of magmas and their derivative cumulates, whereas mantle rocks generally have flat PM-normalised PGE patterns (Hattori and Hart, 1997; Hattori and Shirahase, 1997; Hattori and Guillot, 2007). IPGE fractionation in primitive magmas occur when the degree of mantle melting was not high enough to completely deplete the source of sulfide or alternatively if the primary melt that had previously fractionated Os–Ir-alloys in the magma conduit (Barnes and Fiorentini, 2008; Fiorentini et al., 2011; Gannoun et al., 2016). In contrast, mantle residues usually display systematic PPGE fractionation depending on their degree of melt depletion (e.g., Pearson et al., 2004; Luguet et al., 2007; Maier et al., 2012).

Clearly the Seqi dunites with bulk-rock MgO in excess of 45 wt.% are not primary magmas, and thus the IPGE-depleted dunites likely represent cumulates formed at a late stage where IPGE-alloys had already precipitated. The apparent negative correlation between bulk-rock mg# and Ir (and Os) abundances suggest that IPGE-rich alloys did not saturate until after the earliest formed olivine (Fig. D7 in Appendix D). Bulk-rock mg# is clearly controlled by the addition of cumulus chromite (Fig. 11), and there is also a strong positive correlation between IPGE contents and the chromite abundance of the different Seqi samples (Fig. D7 in Appendix D). This is especially obvious if also considering the chromitite samples. This affinity of certain PGEs for chromite is a common feature of fractional crystallisation that is observed in a range of different magma types (Ballhaus, 1998; Pagé and Barnes, 2016).

Komatiites tend to have slightly positive slopes on a PM-normalised PGE diagrams due to the more incompatible nature of the PPGEs (platinum-affinity PGES) than the IPGEs, however their derivative cumulates have essentially flat patterns (Fiorentini et al., 2011). This is unlike the Seqi rocks, which have slightly negative slopes and thus low Pd/Ru ratios and lower Cu abundances than komatiites and their associated cumulates. It should be noted that the positive Au-anomaly is a feature that is also observed for komatiite cumulates, however, overall the vastly different Ni/Cu, Al_2O_3/TiO_2 in combination with the U-shaped trace element patterns (elevated Th and lower Gd_N/Yb_N ratios), suggest that the Seqi Ultramafic Complex was not derived from a komatiitic primary magma. However, we note that plutonic ultramafic rocks (dunite) associated with Phanerozoic komatiites on Gorgona Island in the Caribbean have been interpreted by Révillon et al. (2000) to represent the plumbing system (magma conduit) of an oceanic

plateau. A similar interpretation of the Seqi Ultramafic Complex appears feasible as we will point out in Section 6.3 below.

6.2. Mineral compositional fingerprints

Although it is possible that the Seqi peridotites experienced serpentinisation at some point (e.g., during early crustal accretion) and later prograde olivine growth during granulite-facies metamorphism, there are a number of arguments against this: (1) the preservation of apparent primary igneous layering and slump textures in chromitite; (2) the high Al-content of olivine cores, which preserves magmatic temperatures (Section 5.7); and (3) the low αH_2O conditions constrained by peak metamorphism would be incompatible with prograde metamorphism from a completely hydrated protolith.

Mg–Fe exchange thermometers do document redistribution of Mg and Fe during metamorphism among spinel, olivine and orthopyroxene, but given the dry conditions, this is interpreted to largely take place under closed system conditions and be confined to mineral rims and smaller grains. The temperatures that are recorded by spinel–olivine Fe–Mg exchange and by Al–Cr in orthopyroxene are not consistent as explained in Section 5.7. The latter system records temperatures that correspond well with the observed mineralogy with an assemblage of olivine + orthopyroxene + tremolite in the peridotites, which would place the metamorphic conditions of these rocks at a temperature above 700 °C.

As mentioned previously, calculated bulk-rock mg# of the Seqi rocks is controlled by the modal amount of chromite (Fig. 11a). The left-ward displacement from the 1:1 ratio in Fig. 11a to lower than expected bulk-rock mg# is directly proportional to the normative chromite contents of the rocks, with the homogeneous and porphyritic dunites having less than 0.6 mol% chromite, the layered dunites having between 1.4 mol% and 2.8 mol% chromite, and the peridotites having between 1.0 mol% and 5.4 mol% normative chromite (Section 5.1). This is further evidence that there has been minimal subsolidus re-equilibration between olivine and spinel and that the olivine cores reflects the Mg/Fe ratio of the melt from which they crystallized, regardless of the amount of trapped chromite in these olivine-dominated cumulates. It seems reasonable to assume that the olivine-dominated Seqi rocks preserve their primary igneous olivine compositions with local subsolidus exchange with chromite being limited to spinel rims (Fig. D19 in Appendix D).

The well-established relationship between Fe–Mg exchange of melt and liquid (Roeder and Emslie, 1970), suggest that the most abundant lithological units of the Seqi Ultramafic Complex (layered dunite and homogeneous dunite) with a maximum forsterite content of 93.2, were derived as cumulates from a melt with the liquid-Mg# up to 80.

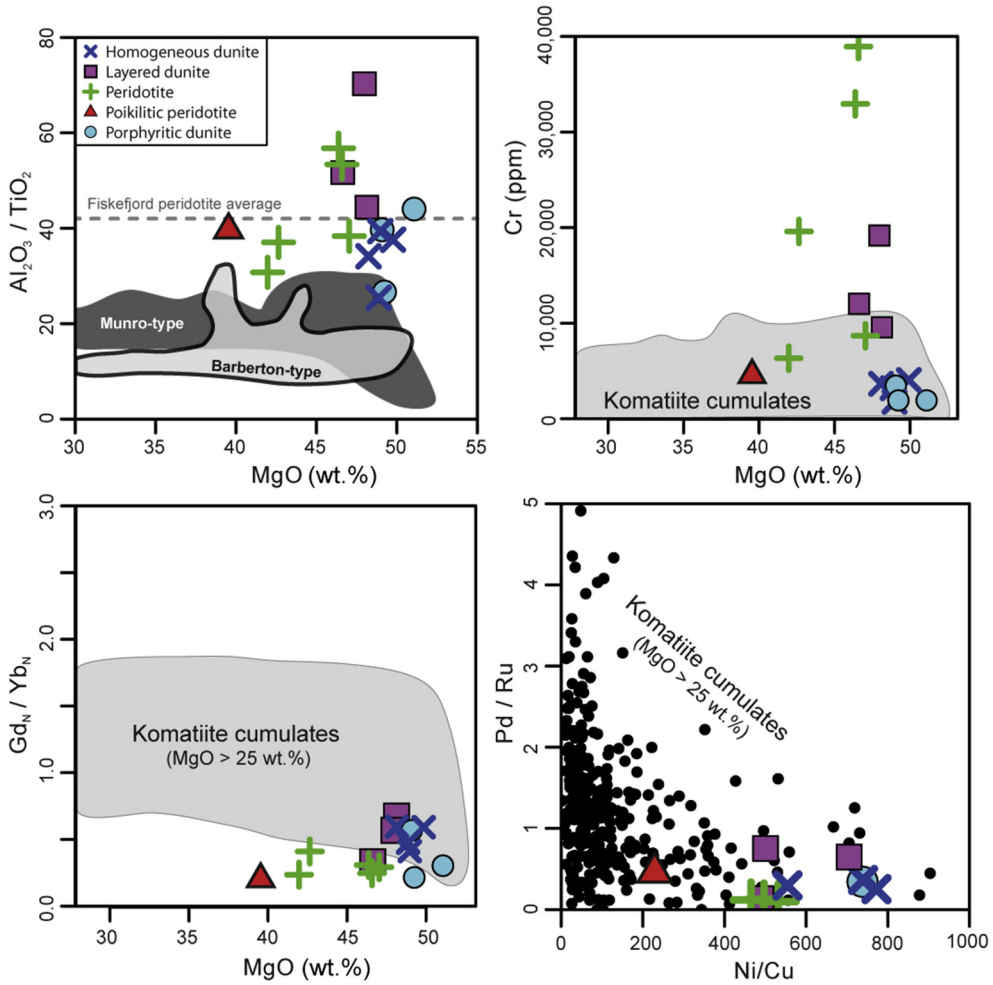

Figure 18. Various plots comparing the different rock types of the Seqi Ultramafic Complex with the bulk-rock compositions of cumulate derived from komatiitic melts. Note that despite the highly forsteritic composition of the Seqi Ultramafic Complex, none of these plots support a komatiitic affinity. The reference komatiite data are from Fiorentini et al. (2011).

The relationship between melt and chromite compositions of Maurel and Maurel (1982), which was further refined by Pagé and Barnes (2009), has been applied to the average Seqi chromitite composition. This calculation suggests a parental melt compositions with approximately 13.0 wt.% Al_2O_3 and 0.4 wt.% TiO_2, which is similar to e.g. Troodos boninites (Cameron, 1985), as also indicated by the U-shaped bulk-rock trace element patterns of the Seqi rocks (Fig. 7). However, the chromite in MORB normalisation of Pagé and Barnes (2009) demonstrates that the Seqi chromitites are not of boninitic affinity (Fig. D32 and D33 in Appendix D), because of that the Seqi chromite is more enriched in Al and Ti, although Mg and Cr are of the right order of magnitude.

Given that the Seqi dunites have undergone granulite-facies metamorphism and textural re-equilibration it is impossible to estimate the initial amount of trapped interstitial liquid in these cumulates. However, intercumulus liquid could potentially explain the U-shaped trace element patterns (Fig. 8), where the most incompatible trace elements are elevated relative to an otherwise positive slope of the HREE (Cawthorn et al., 1992). Nevertheless, given the highly magnesian compositions of olivine and orthopyroxene at Seqi, it would appear unlikely that there was much intercumulus liquid because this would have shifted the Mg# downwards, and required even more magnesian compositions initially (Barnes, 1986).

The bulk-rock major element compositions of the Seqi rocks are adequately accounted for by the measured compositions of olivine, orthopyroxene and spinel (Fig. D34 in Appendix D). Only the metasomatic amphibolite sample (186463) requires a component similar to the analysed amphibole, which likely represents hydrated clinopyroxene as noted above. As a first order constraint on the trace element composition of the melt from which the Seqi cumulates crystallized, the assumption that these rocks represent adcumulates with no significant intercumulus was made and the procedure of Bédard (1994) was tested via trace element inversion. An average composition of the homogeneous dunite and the porphyritic dunites were used, because these are the most common rocks at Seqi and some of the most depleted, which also suggests low levels of trapped interstitial melt. However, the results of the modelling are not consistent with the observed trace element compositions of the Akia terrane, because it would require an extremely trace element enriched parental magma (1000 times chondritic LREE). Thus, either the partition coefficients of Bédard (1994) are not applicable to the conditions under which the Seqi Ultramafic Complex formed (indeed the partition coefficient values of Grégoire et al. (2000) are significantly different), or else significant amounts of trapped interstitial melt were in fact present. Alternatively, the Seqi dunites have experienced a late metasomatic overprint during the intrusion of the regional granitoid crust, which could potentially explain their enrichment in the most incompatible trace elements.

Bulk-rock trace element reconstruction using the measured mineral compositions presented in Section 5.4 is also not capable of accounting for the most incompatible trace elements of Seqi dunites using reasonable estimates of the amount of amphibole and/or trapped melt (Fig. D35 in Appendix D). It would appear that an external component with elevated Th, U, Ta, Nb, Ce, Hf and Zr is needed to balance the trace element budget. However, granitoid crustal contaminant appears unlikely, because it would be depleted in Ta and Nb. It seems more reasonable that the discrepancy between the observed bulk-rock composition of the Seqi dunites and the integrated mineral compositions measured by *in situ* LA-ICP-MS (see Fig. D35 in Appendix D) could be accounted for by fractional liquids in the interstices of the cumulate minerals. Late-stage melts would indeed become enriched in the most incompatible trace elements, and remobilisation of this component would be capable of overprinting the otherwise depleted cumulus phases (Cawthorn et al., 1992).

Orthopyroxene in these rocks may reflect the very high degrees of partial melting of the mantle source region to the point of complete exhaustion, as also proposed for the regional SCLM (Bernstein et al., 2007). Alternatively, orthopyroxene may reflect assimilation of a siliceous component, because it is usually associated with chromitite, which may also have been induced to crystallize by interaction of the primitive magma with crustal material (Irvine, 1977).

The frequent occurrence of orthopyroxene associated with the chromitite bands could either be a secondary feature related to the oxidation of olivine to form magnetite and excess silica during amphibolite-facies metamorphism (Irvine, 1967). The silica would then react with olivine to produce orthopyroxene. Alternatively, the presence of orthopyroxene in association with chromitite could reflect local crustal contamination, which could again add excess silica that would react with olivine to form orthopyroxene. Any silica addition to the magma would also displace the liquid line of descent into the stability field of chromite, which would then crystalize as monomineralic layers (Irvine, 1977).

However, in the above scenario one would expect to see a compositional difference in between orthopyroxene in the dunite and orthopyroxene in the chromitite. However, they are in fact the same, both in terms of major and trace element abundances. Orthopyroxene therefore appears to be the intercumulus phase formed by silica enrichment in the residual trapped liquids. This model would explain the association of orthopyroxene with the chromitites, because spinel takes up no Si and thus pushes the Si content of the intercumulus liquid up even faster than olivine crystallisation would. This could also explain why there is abundant orthopyroxene in the chromitites, when compared to the dunites. Finally, Ni exchange equilibria between orthopyroxene and olivine are identical for the dunites and chromitites (Fig. 17). Thus, orthopyroxene seems to be part of the equilibrium assemblage of the Seqi Ultramafic Complex, if the Ni-thermometry indeed presents only partially reset igneous temperatures, for orthopyroxene to have been an igneous phase (see Section 5.7).

Mössbauer spectroscopic data on the Seqi chromitite yields $Fe^{3+}/\Sigma Fe$ of 0.157–0.209 (rejecting one outlier). This narrow range in composition of chromitite is consistent with the observation that there was no secular evolution in the oxidation state of Earth's mantle according to the recent study by Rollinson et al. (2017). Of the chromitites that were measured by the Mössbauer technique one sample (186469) has significantly higher $Fe^{3+}/\Sigma Fe$ (0.470). Given that most of the electron microprobe data for spinel from the Seqi Ultramafic Complex plot below Fe^{3+}# of 20 (Fig. 19), the more oxidised sample is likely to have been disturbed by either metamorphic fluids (Evans and Frost, 1974), or by metasomatic fluids associated with the intrusion of the hosting granitoids. Lenaz et al. (2014) reported oxidation of chromitites in the mantle section of Oman and ascribed this to an association with ductile shear zones in harzburgite. They estimated the temperature of replacement to be above that of ferritchromite stability but below 700 °C, which would also appear to be reasonable conditions for the metasomatism of parts of the Seqi chromitites. However, it should be stressed that the cores of chromite within the chromitites likely represent the most robust domains of the Seqi Ultramafic Complex, because they would be strongly buffered. Chromite is thus the best potential record of the primary igneous conditions in the Seqi rocks.

The *in situ* trace element data for amphibole in the Seqi rocks displaying negative anomalies for Ta–Nb–Ti (Fig. 13), suggest that it represents igneous clinopyroxene that was later hydrated to form

amphibole during metamorphic hydration. These anomalies are typical for clinopyroxene, but not for igneous amphibole due to significantly lower partition coefficients for these particular trace elements in the latter (e.g., Tiepolo et al., 2007; Otamendi et al., 2016; Terentiev et al., 2016). This interpretation is consistent with the pseudosection modelling (Fig. 17), although further studies of the various settings of amphibole in the Seqi rocks are needed to better constrain the origin of this particular mineral. Regardless of the origin, the negative Sr- and Eu-anomalies of the amphibole points to equilibration with plagioclase, as is also suggested by the bulk-rock trace element data in Fig. 8. This in turn points to a co-magmatic relationship with noritic cumulate rocks that are commonly associated with peridotites in this region (Garde, 1997; Kristensen, 2006; Szilas et al., 2015b).

6.3. Petrogenetic model for the Seqi Ultramafic Complex

Based on the presented data, the Seqi Ultramafic Complex represents a sequence of olivine-dominated cumulates, rather than a mantle fragment. This is supported by the field observations of repeated subparallel layers of chromitite, rhythmic layering and crossbedding of orthopyroxene (Dahl, 2004), the presence of poikilitic orthopyroxene in peridotite, and the overall high modal abundance of chromite (up to 12 vol.%) in the layered dunite, all of which indicates igneous crustal processes that are not typical of mantle sections. As such, Seqi is similar to other mafic-ultramafic intrusions derived from highly magnesian magmas (Barnes, 1989; Wooden et al., 1991; Maier et al., 2000; Harris et al., 2005). The specific chromitite compositions are not compatible with a mantle origin for the Seqi Ultramafic Complex as shown in Fig. 12.

Furthermore, Fig. 19 demonstrates an affinity of the Seqi rocks with reduced layered intrusions based on the overall chromite chemistry. However, we note that Révillon et al. (2000) proposed that plutonic ultramafic rocks (dunites) associated with Phanerozoic komatiites on Gorgona Island, represents the plumbing system of an oceanic plateau. A similar model may in fact also be viable for the Seqi Ultramafic Complex, and this furthermore appears consistent with the observation that supracrustal belts in SW Greenland commonly have cores of ultramafic cumulate rocks (e.g., Polat et al., 2007; Szilas et al., 2014c, 2015a). This model needs further testing, because essentially all of the Archaean supracrustal belts of SW Greenland have been proposed to have formed in a hydrous subduction zone environment (e.g., Polat et al., 2011; Szilas et al., 2013b, 2014b; Furnes et al., 2015). Yet it appears that the parental magma of the Seqi Ultramafic Complex was instead a dry melt derived by large degrees of partial melting of the mantle, and so a direct link is not apparent within the current paradigm for the Archaean of SW Greenland.

Given that the Seqi peridotites (*s.l.*) are not mantle rocks, but consistently have highly forsteritic olivine compositions, it is likely that they represent the first formed cumulates, which were derived by large degree melting of the mantle. The relatively high pressure of emplacement (~2 GPa), yet the complete lack of evidence for true mantle rocks, points to formation of the Seqi Ultramafic Complex by crystal fractionation in the crust rather than in the mantle. An alternative model of critical melting after the exhaustion of garnet in the mantle source (cf., Robin-Popieul et al., 2012) may have relevance for the formation of the parental melt of the Seqi Ultramafic Complex. This could potentially explain the dry and depleted nature of these cumulate rocks, although the viability of this model also needs further detailed investigations to assess. Regardless of the exact parental magma composition and the geotectonic setting, there appears to be robust field and *P–T* evidence for emplacement of the Seqi Ultramafic Complex within thick mafic-ultramafic crust that later underwent partial melting to form the extensive regional TTG-suite crust that presently dominates the craton.

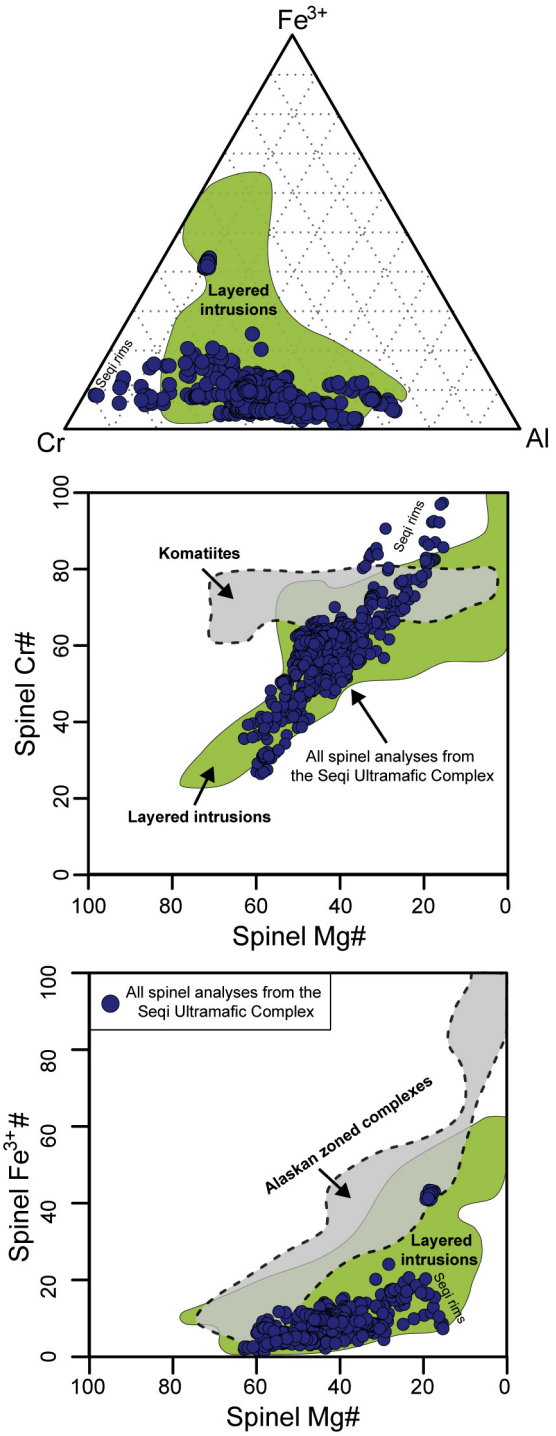

Figure 19. Spinel compositions from all of the Seqi rocks (blue dots) plotted against spinel from three different magma types: (1) layered intrusions, (2) komatiites and (3) Alaskan-type zoned complexes (reference data are from Barnes and Roeder, 2001). As also noted in Fig. 18, komatiites do not have the appropriate characteristics to explain the highly forsteritic rocks of the Seqi Ultramafic Complex. The low Fe^{3+} content of the Seqi spinel is also not compatible with an arc-related origin, such as that of Alaskan-type zoned complexes (Burns, 1985; Thakurta et al., 2008). For clarity, the ranges of spinel from layered intrusions have not been plotted in the two latter diagrams where they essentially overlap with the compositions of the Seqi spinel, thus supporting an affinity of the Seqi Ultramafic Complex with other layered intrusions in general.

Because the first formed olivine is essentially in equilibrium with its mantle source, one would expect that the mantle residue from

which the Seqi magma was extracted would be highly refractory. This is consistent with the observation that much of the North Atlantic Craton is underlain by unusually depleted sub-continental lithospheric mantle (SCLM) and indeed, it is worth noting that similar olivine and spinel compositions are found in mantle xenoliths of the North Atlantic Craton (cf., Bernstein et al., 1998, 2006, 2007, 2013; Wittig et al., 2008, 2010). This remarkably depleted nature of the Archaean SCLM is to be expected given the greater potential temperature of Earth's mantle during the Mesoarchaean Eon (e.g., Herzberg et al., 2010; Ganne and Feng, 2017).

A potential link between the Seqi peridotites and the regional SCLM has recently been proposed based on the highly forsteritic and refractory nature of the Seqi dunites (Pearson et al., 2016; Szilas et al., 2016b), which essentially overlaps in terms of bulk-rock major elements (Fig. D22 in Appendix D), and because the incorporation of cumulate rocks may be able to explain some of the Fe-rich SCLM xenoliths that are unlikely to represent mantle residues. The physical characteristics of the lower crustal Seqi cumulate rocks would indeed be similar to those of the relatively buoyant residual SCLM. Thus, Archaean dunite cumulates may contribute to the long-term development of SCLM by density-driven sorting in the lithospheric mantle in a model similar to that proposed by Arndt et al. (2002) or by Wang et al. (2016). However, in detail there are significant geochemical discrepancies in terms of trace element compositions, as well as of PGE abundances (Figs. D23–D25 in Appendix D) between Seqi-style cumulates and SCLM, which obviously needs to be addressed by future studies.

7. Conclusions

The minimum age of the Seqi Ultramafic Complex is 2970 Ma, as defined by the hosting tonalitic orthogneiss, as well as intrusive sheets of this age. The intrusion of this granitoid crust into the Seqi Ultramafic Complex and has caused fragmentation of the ultramafic body. The peridotites (*s.l.*) of the Seqi Ultramafic Complex consist mainly of dunite and do not represent mantle rocks, but were rather a cumulate that was emplaced into thick mafic crust prior to the formation of the regional TTG-suite crust. A cumulate origin is evident from field observations, the chromite compositions, the highly forsteritic olivine, and the platinum-group element patterns, none of which are comparable to fertile mantle lherzolite, depleted harzburgite or residual mantle dunite. Instead, the Seqi peridotites represent olivine + spinel dominated cumulates, derived from a highly magnesian magma with a relatively high Al/Ti and low Ca/Al ratios.

Mineral parageneses and exchange equilibria suggest emplacement as a relatively dry melt ($\sim\alpha H_2O = 0.1$) at a pressure of less than 2.3 GPa followed by a metamorphic overprint in the mid- to lower-crust at granulate facies conditions (T = 700–900 °C, P = 1.0–2.4 GPa).

In situ LA-ICP-MS trace element data for amphibole in peridotite displays negative Ta–Nb–Ti anomalies. We interpret this to imply metamorphic replacement of clinopyroxene, rather than igneous amphibole, which is in agreement with the reduced and relatively dry conditions suggested by chromite compositions and P–T estimates. However, it is noted that there are several different types and settings of amphibole in the Seqi rocks, which needs further detailed investigations to specifically asses their petrogenesis.

Oxides in the dunite are chromite with variable compositions ranging from Mg# of 15.4 to 62.9 and Cr# ranging from 26.4 to 97.4, whereas chromitite bands found within peridotite have tighter spinel compositions with Mg# ranging from 33.7 to 50.5 and Cr# ranging from 55.7 to 70.1. Spinel Fe^{3+}# is mostly below 20 for all lithological units in the Seqi Ultramafic Complex, which is consistent with Mössbauer spectroscopic data of the chromitite yielding $Fe^{3+}/\Sigma Fe$ of mainly 0.157 to 0.209. The low Fe^{3+}# and moderate Mg# of the Seqi spinel, rule out an origin as an Alaskan-type zoned complex, whereas the high Al/Ti, Ni/Cu and low Gd_N/Yb_N and Pd/Ru are not consistent with a komatiitic affinity either. Thus, bulk-rock major, trace and platinum-group element data does not support a komatiitic affinity of the Seqi rocks, despite their highly forsteritic olivine compositions and an alternative geodynamic setting could be an oceanic plateau.

The Seqi crustal cumulate rocks have negative bulk-rock Eu–Sr-anomalies, which indicates a co-magmatic relationship with noritic cumulate rocks, which are found associated with similar mafic-ultramafic complexes in the Fiskefjord region (Garde, 1997; Kristensen, 2006; Szilas et al., 2015b).

Elevated bulk-rock Th and U in combination with low Nb/La either indicates: (1) crustal contamination of the mantle source region of the primary magma of the Seqi Ultramafic Complex (boninite-style magmatism), or (2) continental crustal assimilation during the intrusion of the Seqi complex into basement that existed prior to the current regional orthogneiss terrane, or (3) alternatively metasomatic overprinting during the late intrusion of the hosting TTG-suite granitoids. These different models are not distinguishable with the currently available geochemical data and thus future isotope studies are needed on these rocks.

Collectively, the highly forsteritic olivine and elevated bulk-rock IPGE abundances point to very hot conditions during the melt extraction from the mantle. The chromite compositions of the Seqi Ultramafic Complex are comparable to those of reduced layered intrusions (or magma conduits). This further suggests that the Seqi cumulates rocks were derived from a primary magma that formed by very large degrees (>40%) of partial melting of the mantle source. We note that such mantle residues could potentially represent the current SCLM of this region, which warrants further investigation to test this possibility, as it could have global implications for the understanding of craton formation.

Acknowledgements

K. Szilas would like to thank Graham Pearson and Tomoaki Morishita for fruitful discussion during fieldwork in Greenland, which helped develop a better understanding of the peridotites of the Fiskefjord region. Jarl Boyd is acknowledged for assistance during the rock sampling at the Seqi Ultramafic Complex. Comments on an early version of the manuscript by Nick Arndt, Ole Dahl, Dmitri Ionov, Troels Nielsen and Marc Norman are appreciated. Editorial handling of the manuscript by Sohini Ganguly is acknowledged. The authors greatly appreciate thorough reviews by Tomoaki Morishita and Riccardo Tribuzio, which significantly improved the resulting paper. Financial support to Kristoffer Szilas from Knud Højgaards Fond for the fieldwork at the Seqi Ultramafic Complex, and research grants VKR023371 from VILLUM FOUNDATION and CF16-0059 from CARLSBERG FOUNDATION made this study possible.

Supplementary data

Supplementary data related to this article can be found at http://dx.doi.org/10.1016/j.gsf.2017.05.003.

References

Arai, T., Omori, S., Komiya, T., Maruyama, S., 2015. Intermediate P/T-type regional metamorphism of the Isua Supracrustal Belt, southern west Greenland: the oldest Pacific-type orogenic belt? Tectonophysics 662, 22–39.

Arndt, N.T., Lewin, É., Albarède, F., 2002. Strange partners: formation and survival of continental crust and lithospheric mantle. Geological Society, London, Special Publications 199, 91–103.

Arndt, N., Lesher, C.M., Barnes, S.J., 2008. Komatiite. Cambridge University Press, New York. ISBN: 978-0521874-748, 488 pp.

Asmund, G., Boertmann, D., Johansen, P., 2009. Baseline and Monitoring Studies at the Seqi Mine 2004 to 2007. National Environmental Research Institute, NERI Technical Report No. 715, Aarhus University, Denmark, 90 pp.
Ballhaus, C., Berry, R.F., Green, D.H., 1991. High pressure experimental calibration of the olivine–orthopyroxene–spinel oxygen geobarometer: implications for the oxidation state of the mantle. Contributions to Mineralogy and Petrology 107, 27–40.
Ballhaus, C., 1998. Origin of podiform chromite deposits by magma mingling. Earth and Planetary Science Letters 156, 185–193.
Barnes, S.J., 1986. The effect of trapped liquid crystallization on cumulus mineral compositions in layered intrusions. Contributions to Mineralogy and Petrology 93, 524–531.
Barnes, S.J., Fiorentini, M.L., 2008. Iridium, ruthenium and rhodium in komatiites: evidence for iridium alloy saturation. Chemical Geology 257, 44–58.
Barnes, S.J., 1989. Are Bushveld U-type parent magmas boninites or contaminated komatiites? Contributions to Mineralogy and Petrology 101, 447–457.
Barnes, S.J., Roeder, P.L., 2001. The range of spinel compositions in terrestrial mafic and ultramafic rocks. Journal of Petrology 42, 2279–2302.
Becker, H., Horan, M.F., Walker, R.J., Gao, S., Lorand, J.P., Rudnick, R.L., 2006. Highly siderophile element composition of the Earth's primitive upper mantle: constraints from new data on peridotite massifs and xenoliths. Geochimica et Cosmochimica Acta 70, 4528–4550.
Bédard, J.H., 1994. A procedure for calculating the equilibrium distribution of trace elements among the minerals of cumulate rocks, and the concentration of trace elements in the coexisting liquids. Chemical Geology 118, 143–153.
Begg, G.C., Hronsky, J.A., Arndt, N.T., Griffin, W.L., O'Reilly, S.Y., Hayward, N., 2010. Lithospheric, cratonic, and geodynamic setting of Ni-Cu-PGE sulfide deposits. Economic Geology 105, 1057–1070.
Bennett, V.C., Nutman, A.P., Esat, T.M., 2002. Constraints on mantle evolution from $^{187}Os/^{188}Os$ isotopic compositions from Archaean ultramafic rocks from southern west Greenland (3.8 Ga) and western Australia (3.46 Ga). Geochimica et Cosmochimica Acta 66, 2615–2630.
Bernstein, S., Kelemen, P.B., Brooks, C.K., 1998. Depleted spinel harzburgite xenoliths in Tertiary dykes from East Greenland: restites from high degree melting. Earth and Planetary Science Letters 154, 221–235.
Bernstein, S., Hanghøj, K., Kelemen, P.B., Brooks, C.K., 2006. Ultra-depleted, shallow cratonic mantle beneath West Greenland: dunitic xenoliths from Ubekendt Ejland. Contributions to Mineralogy and Petrology 152, 335–347.
Bernstein, S., Kelemen, P.B., Hanghøj, K., 2007. Consistent olivine Mg# in cratonic mantle reflects Archean mantle melting to the exhaustion of orthopyroxene. Geology 35, 459–462.
Bernstein, S., Szilas, K., Kelemen, P.B., 2013. Highly depleted cratonic mantle in West Greenland extending into diamond stability field in the Proterozoic. Lithos 168, 160–172.
Bodinier, J.L., Godard, M., 2003. Orogenic, ophiolitic, and abyssal peridotites. Treatise on Geochemistry 2, 568 pp.
Bridgwater, D., McGregor, V.R., Myers, J.S., 1974. A horizontal tectonic regime in the Archaean of Greenland and its implications for early crustal thickening. Precambrian Research 1, 179–197.
Brey, G.P., Köhler, T., 1990. Geothermobarometry in four-phase Lherzolites II. New thermobarometers and practical assessment of existing thermobarometers. Journal of Petrology 31, 1353–1378.
Burns, L.E., 1985. The Border Ranges ultramafic and mafic complex, south-central Alaska: cumulate fractionates of island-arc volcanics. Canadian Journal of Earth Sciences 22, 1020–1038.
Cameron, E.N., 1978. The lower zone of the eastern Bushveld Complex in the Olifants River trough. Journal of Petrology 19, 437–462.
Cameron, W.E., 1985. Petrology and origin of primitive lavas from the Troodos ophiolite, Cyprus. Contributions to Mineralogy and Petrology 89, 239–255.
Cawthorn, R.G., Sander, B.K., Jones, I.M., 1992. Evidence for the trapped liquid shift effect in the Mount Ayliff Intrusion, South Africa. Contributions to Mineralogy and Petrology 111, 194–202.
Cawthorn, R.G. (Ed.), 1996. Layered Intrusions. Elsevier, New York, 531 pp.
Christiansen, O., 1997. The Seqinnersuuaq Olivine Deposit Southern West Greenland – a Review of Geological and Technical Information. NunaOil A/S company report. GEUS report file 21628, 137 pp.
Christiansen, O., 1998. The Seqinnersuuaq Olivine Deposit Southern West Greenland – Preliminary Magnetic Separation Tests. NunaOil A/S company report. GEUS report file 21625, 8 pp.
Colás, V., Gonzalez-Jimenez, J.M., Griffin, W.L., Fanlo, I., Gervilla, F., O'Reilly, S.Y., Pearson, N.J., Kerestedjian, T., Proenza, J.A., 2014. Fingerprints of metamorphism in chromite: new insights from minor and trace elements. Chemical Geology 389, 137–152.
Connolly, J.A.D., 2005. Computation of phase equilibria by linear programming: a tool for geodynamic modeling and its application to subduction zone decarbonation. Earth and Planetary Science Letters 236, 524–541.
Dahl, O., 2004. Seqi Olivine Deposit Report 2003. Crew Gold Corporation report for Bureau of Minerals and Petroleum (BMP), 94 pp.
DeBari, S.M., Coleman, R.G., 1989. Examination of the deep levels of an island arc: evidence from the Tonsina Ultramafic–Mafic Assemblage, Tonsina, Alaska. Journal of Geophysical Research: Solid Earth 94, 4373–4391.
de Hoog, J.C.M., Gall, L., Cornell, D.H., 2010. Trace-element geochemistry of mantle olivine and application to mantle petrogenesis and geothermobarometry. Chemical Geology 270, 196–215.
Diener, J., Powell, R., 2012. Revised activity–composition models for clinopyroxene and amphibole. Journal of Metamorphic Geology 30, 131–142.
Downes, H., 2001. Formation and modification of the shallow sub-continental lithospheric mantle: a review of geochemical evidence from ultramafic xenolith suites and tectonically emplaced ultramafic massifs of western and central Europe. Journal of Petrology 42, 233–250.
Dyck, B., Reno, B.L., Kokfelt, T.F., 2015. The Majorqaq Belt: a record of Neoarchaean orogenesis during final assembly of the North Atlantic Craton, southern West Greenland. Lithos 220, 253–271.
Dziggel, A., Diener, J.F.A., Kolb, J., Kokfelt, T.F., 2014. Metamorphic record of accretionary processes during the Neoarchaean: the Nuuk region, southern West Greenland. Precambrian Research 242, 22–38.
Eales, H.V., Cawthorn, R.G., 1996. The bushveld complex. Developments in Petrology 15, 181–229.
Evans, B.W., Frost, B.R., 1974. Chrome-spinel in progressive metamorphism – a preliminary analysis. Geochimica et Cosmochimica Acta 39, 959–972.
Fiorentini, M.L., Barnes, S.J., Maier, W.D., Burnham, O.M., Heggie, G., 2011. Global variability in the platinum-group element contents of komatiites. Journal of Petrology 52, 83–112.
Frei, D., Gerdes, A., 2009. Precise and accurate in situ U–Pb dating of zircon with high sample throughput by automated LA-SF-ICP-MS. Chemical Geology 261, 261–270.
Friend, C.R.L., Bennett, V.C., Nutman, A.P., 2002. Abyssal peridotites >3800 Ma from southern west Greenland: field relationships, petrography, geochronology, whole-rock and mineral chemistry of dunite and harzburgite inclusions in the Itsaq Gneiss Complex. Contributions to Mineralogy and Petrology 143, 71–92.
Friend, C.R., Nutman, A.P., 2005. New pieces to the Archaean terrane jigsaw puzzle in the Nuuk region, southern West Greenland: steps in transforming a simple insight into a complex regional tectonothermal model. Journal of the Geological Society 162, 147–162.
Friend, C.R., Nutman, A.P., 2010. Eoarchean ophiolites? New evidence for the debate on the Isua supracrustal belt, southern West Greenland. American Journal of Science 310, 826–861.
Furnes, H., Dilek, Y., De Wit, M., 2015. Precambrian greenstone sequences represent different ophiolite types. Gondwana Research 27, 649–685.
Ganne, J., Feng, X., 2017. Primary magmas and mantle temperatures through time. Geochemistry, Geophysics, Geosystems 18, 2016GC006787.
Gannoun, A., Burton, K.W., Day, J.M., Harvey, J., Schiano, P., Parkinson, I., 2016. Highly siderophile element and Os isotope systematics of volcanic rocks at divergent and convergent plate boundaries and in intraplate settings. Reviews in Mineralogy and Geochemistry 81, 651–724.
Garde, A.A., 1997. Accretion and evolution of an Archaean high-grade grey gneiss–amphibolite complex: the Fiskefjord area, southern West Greenland. Geology of Greenland Survey Bulletin 177, 115 pp.
Garde, A.A., 2007. A mid-Archaean island arc complex in the eastern Akia terrane, Godthåbsfjord, southern West Greenland. Journal of the Geological Society 164, 565–579.
Garde, A.A., Whitehouse, M., Christensen, R., 2012. Mesoarchean epithermal gold mineralization preserved at upper amphibolite-facies grade, Qussuk, southern West Greenland. Economic Geology 107, 881–908.
Garde, A.A., Dyck, B., Esbensen, K.H., Johansson, L., Möller, C., 2015. The Finnefjeld domain, Maniitsoq structure, West Greenland: differential rheological features and mechanical homogenisationin response to impacting? Precambrian Research 255, 791–808.
Gerdes, A., Zeh, A., 2006. Combined U-Pb and Hf isotope LA-(MC)-ICP-MS analyses of detrital zircons: comparison with SHRIMP and new constraints for the provenance and age of an Armorican metasediment in Central Germany. Earth and Planetary Science Letters 249, 47–61.
Grégoire, M., Moine, B.N., O'Reilly, S.Y., Giret, A., 2000. Trace element residence and partitioning in mantle xenoliths metasomatized by highly alkaline, silicate- and carbonate-rich melts (Kerguelen Islands, Indian Ocean). Journal of Petrology 41, 477–509.
Groves, D.I., Bierlein, F.P., 2007. Geodynamic settings of mineral deposit systems. Journal of the Geological Society 164, 19–30.
Hanghøj, K., Kelemen, P.B., Hassler, D., Godard, M., 2010. Composition and genesis of depleted mantle peridotites from the Wadi Tayin Massif, Oman Ophiolite; major and trace element geochemistry, and Os isotope and PGE systematics. Journal of Petrology 51, 201–227.
Hanmer, S., Greene, D.C., 2002. A modern structural regime in the Paleoarchean (~3.64 Ga); Isua Greenstone Belt, southern West Greenland. Tectonophysics 346, 201–222.
Harris, C., Pronost, J.J., Ashwal, L.D., Cawthorn, R.G., 2005. Oxygen and hydrogen isotope stratigraphy of the Rustenburg Layered Suite, Bushveld Complex: constraints on crustal contamination. Journal of Petrology 46, 579–601.
Hattori, K., Hart, S.R., 1997. PGE and Os isotopic signatures for ultramafic rocks from the base of the Talkeetna island arc, Alaska. EOS 78, 339.
Hattori, K., Shirahase, T., 1997. Platinum group elements and osmium isotope signatures of the Kohistan island arc sequence, Himalaya-Karakaram area. EOS 78, 829.
Hattori, K.H., Guillot, S., 2007. Geochemical character of serpentinites associated with high-to ultrahigh-pressure metamorphic rocks in the Alps, Cuba, and the Himalayas: recycling of elements in subduction zones. Geochemistry, Geophysics, Geosystems 8, 2007GC001594.
Hawthorne, F.C., Oberti, R., Harlow, G.E., Maresch, W.V., Martin, R.F., Schumacher, J.C., Welch, M.D., 2012. Nomenclature of the amphibole supergroup. American Mineralogist 97, 2031–2048.

Herzberg, C., Condie, K., Korenaga, J., 2010. Thermal history of the Earth and its petrological expression. Earth and Planetary Science Letters 292, 79–88.
Holland, T.J.B., Powell, R., 2011. An improved and extended internally consistent thermodynamic dataset for phases of petrological interest, involving a new equation of state for solids. Journal of Metamorphic Geology 29, 333–383.
Huber, H., Koeberl, C., McDonald, I., Reimold, W.U., 2001. Geochemistry and petrology of Witwatersrand and Dwyka diamictites from South Africa: search for an extraterrestrial component. Geochimica et Cosmochimica Acta 65, 2007–2016.
Irvine, T.N., 1967. Chromian spinel as a petrogenetic indicator. Part 2. Petrologic applications. Canadian Journal of Earth Sciences 4, 71–103.
Irvine, T.N., 1974. Petrology of the Duke Island ultramafic complex southeastern Alaska. Geological Society of America Memoirs 138, 1–244.
Irvine, T.N., 1977. Origin of chromitite layers in the Muskox intrusion and other stratiform intrusions: a new interpretation. Geology 5, 273–277.
Jackson, S., Pearson, N.J., Griffin, W.L., Belousova, E.A., 2004. The application of laser ablation – inductively coupled plasma – mass spectrometry to in situ U–Pb zircon geochronology. Chemical Geology 211, 47–69.
Janošek, V., Farrow, C.M., Erban, V., 2006. Interpretation of whole-rock geochemical data in igneous geochemistry: introducing Geochemical Data Tool (GCDkit). Journal of Petrology 47, 1255–1259.
Jenner, F.E., Bennett, V.C., Nutman, A.P., Friend, C.R.L., Norman, M.D., Yaxley, G., 2009. Evidence for subduction at 3.8 Ga: geochemistry of arc-like metabasalts from the southern edge of the Isua Supracrustal Belt. Chemical Geology 261, 83–98.
Jenner, F., Bennett, V., Yaxley, G., Friend, C., Nebel, O., 2014. Eoarchean within-plate basalts from southwest Greenland. Geology 42, 331–331.
Jennings, E.S., Holland, T.J.B., 2015. A simple thermodynamic model for melting of peridotite in the system NCFMASOCr. Journal of Petrology 56, 869–892.
Kelemen, P.B., Dick, H.J.B., Quick, J.E., 1992. Formation of harzburgite by pervasive melt/rock reaction in the upper mantle. Nature 358, 635–641.
Keulen, N., Schumacher, J.C., Næraa, T., Kokfelt, T.F., Scherstén, A., Szilas, K., van Hinsberg, V.J., Schlatter, D.M., Windley, B.F., 2014. Meso-and Neoarchaean geological history of the Bjørnesund and Ravns Storø Supracrustal Belts, southern West Greenland: settings for gold enrichment and corundum formation. Precambrian Research 254, 36–58.
Kisters, A.F.M., van Hinsberg, V.J., Szilas, K., 2012. Geology of an Archaean accretionary complex – the structural record of burial and return flow in the Tartoq Group of South West Greenland. Precambrian Research 220, 107–122.
Kolb, J., Kokfelt, T.F., Dziggel, A., 2012. Geodynamic setting and deformation history of an Archaean terrane at mid-crustal level: the Tasiusarsuaq terrane of southern West Greenland. Precambrian Research 212, 34–56.
Kristensen, T., 2006. En geologisk og geokemisk tolkning af mafiske og ultramafiske bjergarter og deres økonomiske mineralpotentiale, Fiskefjordsregionen, sydlige Vestgrønland. Unpublished M.Sc. thesis. Aarhus University, 135 pp.
Kusky, T.M., Li, J.H., Tucker, R.D., 2001. The Archean Dongwanzi ophiolite complex, North China Craton: 2.505-billion-year-old oceanic crust and mantle. Science 292, 1142–1145.
Le Maitre, R.W., Streckeisen, A., Zanettin, B., Le Bas, M.J., Bonin, B., Bateman, P. (Eds.), 2005. Igneous Rocks: A Classification and Glossary of Terms: Recommendations of the International Union of Geological Sciences Subcommission on the Systematics of Igneous Rocks. Cambridge University Press, 254 pp.
Lenaz, D., Adetunji, J., Rollinson, H., 2014. Determination of $Fe^{3+}/\Sigma Fe$ ratios in chrome spinels using a combined Mössbauer and single-crystal X-ray approach: application to chromitites from the mantle section of the Oman ophiolite. Contributions to Mineralogy and Petrology 167, 1–17.
Liermann, H.P., Ganguly, J., 2003. Fe-Mg fractionation between orthopyroxene and spinel: experimental calibration in the system $FeO–MgO–Al_2O_3–Cr_2O_3–SiO_2$, and applications. Contributions to Mineralogy and Petrology 145, 217–227.
Lindsley, D.H., 1983. Pyroxene thermometry. American Mineralogist 68, 477–493.
Lindsley, D.H., Andersen, D.J., 1983. A two-pyroxene thermometer. Journal of Geophysical Research: Solid Earth 88 (S02).
Ludwig, K.R., 2012. Using Isoplot/Ex, version 3.76, a geochronological toolkit for Microsoft Excel. Berkeley Geochronology Center Special Pubublication 6.
Luguet, A., Shirey, S.B., Lorand, J.P., Horan, M.F., Carlson, R.W., 2007. Residual platinum-group minerals from highly depleted harzburgites of the Lherz massif (France) and their role in HSE fractionation of the mantle. Geochimica et Cosmochimica Acta 71, 3082–3097.
McBirney, A.R., 1996. The Skaergaard intrusion. Developments in Petrology 15, 147–180.
McDonald, I., Viljoen, K.S., 2013. Platinum-group element geochemistry of mantle eclogites: a reconnaissance study of xenoliths from the Orapa kimberlite, Botswana. Applied Earth Science: Transactions of the Institutions of Mining and Metallurgy, Section B 115, 81–93.
Mai, H.N., 1998. Seqinnersuuaq olivine deposit – pre-feasibility study, technical description and cost estimation. NunaOil A/S company report. GEUS report file 21627, 27 pp.
Maier, W.D., Arndt, N.T., Curl, E.A., 2000. Progressive crustal contamination of the Bushveld Complex: evidence from Nd isotopic analyses of the cumulate rocks. Contributions to Mineralogy and Petrology 140, 316–327.
Maier, W.D., 2005. Platinum-group element (PGE) deposits and occurrences: mineralization styles, genetic concepts, and exploration criteria. Journal of African Earth Sciences 41, 165–191.
Maier, W.D., Peltonen, P., McDonald, I., Barnes, S.J., Barnes, S.J., Hatton, C., Viljoen, F., 2012. The concentration of platinum-group elements and gold in southern African and Karelian kimberlite-hosted mantle xenoliths: implications for the noble metal content of the Earth's mantle. Chemical Geology 302–303, 119–135.
Mathison, C.I., Ahmat, A.L., 1996. The Windimurra Complex, Western Australia. Developments in Petrology 15, 485–510.
Maurel, C., Maurel, P., 1982. Experimental study of the solubility of chromium in basic silicate melts and its distribution between liquid and coexistant minerals – conditions of existence of chromian spinel. Bulletin de Mineralogie 105, 640–647.
McBirney, A.R., Noyes, R.M., 1979. Crystallization and layering of the Skaergaard intrusion. Journal of Petrology 20, 487–554.
McCallum, I.S., 1996. The stillwater complex. Developments in Petrology 15, 441–483.
McCallum, I.S., Raedeke, L.D., Mathez, E.A., 1980. Investigations of the Stillwater Complex: Part I. Stratigraphy and structure of the banded zone. American Journal of Science 280, 59–87.
Myers, J.S., 1976. Channel deposits of peridotite, gabbro and chromitite from turbidity currents in the stratiform Fiskenæsset anorthosite complex, southwest Greenland. Lithos 9, 281–291.
Naldrett, A.J., 1999. World-class Ni-Cu-PGE deposits: key factors in their genesis. Mineralium Deposita 34, 227–240.
Nielsen, T.F., Andersen, J.Ø., Holness, M.B., Keiding, J.K., Rudashevsky, N.S., Rudashevsky, V.N., Veksler, I.V., 2015. The Skaergaard PGE and gold deposit: the result of in situ fractionation, sulphide saturation, and magma chamber-scale precious metal redistribution by immiscible Fe-rich melt. Journal of Petrology 56, 1643–1676.
Niu, Y., 2004. Bulk-rock major and trace element compositions of abyssal peridotites: implications for mantle melting, melt extraction and post-melting processes beneath mid-ocean ridges. Journal of Petrology 45, 2423–2458.
Nutman, A.P., McGregor, V.R., Friend, C.R.L., Bennett, V.C., Kinny, P.D., 1996. The Itsaq Gneiss Complex of southern West Greenland; the world's most extensive record of early crustal evolution (3900–3600 Ma). Precambrian Research 78, 1–39.
Nutman, A.P., Friend, C.R., 2007. Adjacent terranes with ca. 2715 and 2650 Ma high-pressure metamorphic assemblages in the Nuuk region of the North Atlantic Craton, southern West Greenland: complexities of Neoarchaean collisional orogeny. Precambrian Research 155, 159–203.
Otamendi, J.E., Tiepolo, M., Walker, B.A., Cristofolini, E.A., Tibaldi, A.M., 2016. Trace elements in minerals from mafic and ultramafic cumulates of the central Sierra de Valle Fértil, Famatinian arc, Argentina. Lithos 240, 355–370.
Pagé, P., Barnes, S.J., 2009. Using trace elements in chromites to constrain the origin of podiform chromitites in the Thetford Mines ophiolite, Québec, Canada. Economic Geology 104, 997–1018.
Pagé, P., Barnes, S.J., 2016. The influence of chromite on osmium, iridium, ruthenium and rhodium distribution during early magmatic processes. Chemical Geology 420, 51–68.
Pal, T., Moon, H., Mitra, S., 1994. Distribution of iron cations in natural chromites at different stages of oxidation – a ^{57}Fe Mössbauer investigation. Journal of Geological Society of India 44, 53–64.
Palme, H., O'Neill, H.C., 2003. Compositional estimates of mantle composition. In: Carlson, R.W. (Ed.), The Mantle and Core, Vol. 2. In: Holland, H.D., Turekian, K.K. (Eds.), Treatise on Geochemistry. Elsevier-Pergamon, Oxford, UK, pp. 1–38.
Paton, C., Hellstrom, J., Paul, B., Woodhead, J., Hergt, J., 2011. Iolite: freeware for the visualisation and processing of mass spectrometric data. Journal of Analytical Atomic Spectrometry 26, 2508–2518.
Pearson, D.G., Irvine, G.J., Ionov, D.A., Boyd, F.R., Dreibus, G.E., 2004. Re–Os isotope systematics and platinum group element fractionation during mantle melt extraction: a study of massif and xenolith peridotite suites. Chemical Geology 208, 29–59.
Pearson, D.G., Wang, H., van Hunen, J., Szilas, K., 2016. Making the Complex Mantle Keels Beneath Cratons. Goldschmidt Conference, Yokohama. https://goldschmidt.info/2016///uploads/abstracts/finalPDFs/2457.pdf.
Petrus, J.A., Kamber, B.S., 2012. VizualAge: a novel approach to laser ablation ICP-MS U-Pb geochronology data reduction. Geostandards and Geoanalytical Research 36, 247–270.
Polat, A., Hofmann, A.W., Rosing, M.T., 2002. Boninite-like volcanic rocks in the 3.7–3.8 Ga Isua greenstone belt, West Greenland: geochemical evidence for intra-oceanic subduction zone processes in the early Earth. Chemical Geology 184, 231–254.
Polat, A., Appel, P.W., Frei, R., Pan, Y., Dilek, Y., Ordóñez-Calderón, J.C., Raith, J.G., 2007. Field and geochemical characteristics of the Mesoarchean (~3075Ma) Ivisaartoq greenstone belt, southern West Greenland: evidence for seafloor hydrothermal alteration in supra-subduction oceanic crust. Gondwana Research 11, 69–91.
Polat, A., Appel, P.W., Fryer, B.J., 2011. An overview of the geochemistry of Eoarchean to Mesoarchean ultramafic to mafic volcanic rocks, SW Greenland: implications for mantle depletion and petrogenetic processes at subduction zones in the early Earth. Gondwana Research 20, 255–283.
Polat, A., Wang, L., Appel, P.W., 2015. A review of structural patterns and melting processes in the Archean craton of West Greenland: evidence for crustal growth at convergent plate margins as opposed to non-uniformitarian models. Tectonophysics 662, 67–94.
Povdin, P., 1988. Ni–Mg partitioning between synthetic olivines and orthopyroxene: applications to geothermometry. American Mineralogist 73, 274–280.
Prescher, C., McCammon, C., Dubrovinsky, L., 2012. MossA: a program for analyzing energy-domain Mössbauer spectra from conventional and synchrotron sources. Journal of Applied Crystallography 45, 329–331.

Quintiliani, M., 2005. Fe-57 Mossbauer spectroscopy analysis of spinels: Fe^{3+}/Fe-tot quantification accuracy and consequences on $f(O_2)$ estimate. Periodico di Mineralogia 74, 139–146.
Rais, A., Yousif, A.A., Al-shihi, M.H., Al-rawas, A.D., Gismelseed, A.M., El-zain, M.E., 2003. Cation distribution and magnetic properties of natural chromites. Physica Status Solidi (b) 239, 439–446.
Révillon, S., Arndt, N.T., Chauvel, C., Hallot, E., 2000. Geochemical study of ultramafic volcanic and plutonic rocks from Gorgona Island, Colombia: the plumbing system of an oceanic plateau. Journal of Petrology 41, 1127–1153.
Robin-Popieul, C.C., Arndt, N.T., Chauvel, C., Byerly, G.R., Sobolev, A.V., Wilson, A., 2012. A new model for Barberton komatiites: deep critical melting with high melt retention. Journal of Petrology 53, 2191–2229.
Roeder, P.L., Emslie, R., 1970. Olivine-liquid equilibrium. Contributions to Mineralogy and Petrology 29, 275–289.
Rollinson, H., Appel, P.W.U., Frei, R., 2002. A metamorphosed, Early Archaean chromitites from West Greenland: implications for the genesis of Archaean anorthositic chromitites. Journal of Petrology 43, 2143–2170.
Rollinson, H., 2005. Chromite in the mantle section of the Oman ophiolite: a new genetic model. Island Arc 14, 542–550.
Rollinson, H., 2007. Recognising early Archaean mantle: a reappraisal. Contributions to Mineralogy and Petrology 154, 241–252.
Rollinson, H.R., Adetunji, J., Yousif, A.A., Gismelseed, A.M., 2012. New Mössbauer measurements of $Fe^{3+}/\Sigma Fe$ in chromites from the mantle section of the Oman ophiolite: evidence for the oxidation of the sub-oceanic mantle. Mineralogical Magazine 76, 596–597.
Rollinson, H.R., Adetunji, J., Lenaz, D., Szilas, K., 2017. Archaean chromitites show constant $Fe^{3+}/\Sigma Fe$ in Earth's asthenospheric mantle since 3.8 Ga. Lithos 282, 316–325.
Rosengren, N.M., Beresford, S.W., Grguric, B.A., Cas, R.A.F., 2005. An intrusive origin for the komatiitic dunite-hosted Mount Keith disseminated nickel sulfide deposit, Western Australia. Economic Geology 100, 149–156.
Søndergaard, J., Schiedek, D., Asmund, G., 2009. Environmental Monitoring at the Seqi Olivine Mine 2008–2009. National Environmental Research Institute, Aarhus University, 42 pp.
Spandler, C., Mavrogenes, J., Arculus, R., 2005. Origin of chromitites in layered intrusions: evidence from chromite-hosted melt inclusions from the Stillwater Complex. Geology 33, 893–896.
Streckeisen, A., 1973. Plutonic rocks: classification and nomenclature recommended by the IUGS subcommission on the systematics of igneous rocks. Geotimes 18, 26–30.
Streckeisen, A., 1976. To each plutonic rock its proper name. Earth-Science Reviews 12, 1–33.
Szilas, K., van Hinsberg, V.J., Kisters, A.F.M., Kokfelt, T.F., Scherstén, A., Windley, B.F., 2011. Remnants of Mesoarchaean oceanic crust in the Tartoq Group, South-West Greenland. Geological Survey of Denmark and Greenland Bulletin 23, 57–60.
Szilas, K., Næraa, T., Scherstén, A., Stendal, H., Frei, R., van Hinsberg, V.J., Kokfelt, T.F., Rosing, M.T., 2012a. Origin of Mesoarchaean arc-related rocks with boninite/komatiite affinities from southern West Greenland. Lithos 144, 24–39.
Szilas, K., Hoffmann, J.E., Scherstén, A., Rosing, M.T., Windley, B.F., Kokfelt, T.F., Keulen, N., van Hinsberg, V.J., Næraaa, T., Frei, R., Münker, C., 2012b. Complex calc-alkaline volcanism recorded in Mesoarchaean supracrustal belts north of Frederikshåb Isblink, southern West Greenland: implications for subduction zone processes in the early Earth. Precambrian Research 208, 90–123.
Szilas, K., Hoffmann, J., Scherstén, A., Kokfelt, T.F., Münker, C., 2013a. Archaean andesite petrogenesis: insights from the Grædefjord Supracrustal Belt, southern West Greenland. Precambrian Research 236, 1–15.
Szilas, K., van Hinsberg, V.J., Kisters, A.F.M., Hoffmann, J.E., Kokfelt, T.F., Scherstén, A., Windley, B.F., Münker, C., 2013b. Remnants of arc-related Mesoarchaean oceanic crust in the Tartoq Group, SW Greenland. Gondwana Research 23, 436–451.
Szilas, K., Hoffmann, J.E., Münker, C., Dziggel, A., Rosing, M.T., 2014a. Eoarchean within-plate basalts from southwest Greenland: comment. Geology 42 e330–e330.
Szilas, K., van Gool, J.A.M., Scherstén, A., Frei, R., 2014b. The Mesoarchaean Storø Supracrustal Belt, Nuuk region, southern West Greenland: an arc-related basin with continent-derived sedimentation. Precambrian Research 247, 208–222.
Szilas, K., van Hinsberg, J., Creaser, R., Kisters, A.F.M., 2014c. The geochemical composition of serpentinites in the Mesoarchaean Tartoq Group, SW Greenland: harzburgitic cumulates or melt-modified mantle? Lithos 198, 103–116.
Szilas, K., Kelemen, P.B., Rosing, M.T., 2015a. The petrogenesis of ultramafic rocks in the >3.7 Ga Isua supracrustal belt, southern West Greenland: geochemical evidence for two distinct magmatic cumulate trends. Gondwana Research 28, 565–580.
Szilas, K., Kelemen, P.B., Bernstein, S., 2015b. Peridotite enclaves hosted by Mesoarchaean TTG-suite orthogneisses in the Fiskefjord region of southern West Greenland. GeoResJ 7, 22–34.
Szilas, K., Maher, K., Bird, D.K., 2016a. Aluminous gneiss derived by weathering of basaltic source rocks in the Neoarchean Storø Supracrustal Belt, southern West Greenland. Chemical Geology 441, 63–80.
Szilas, K., Tusch, J., Hoffmann, J.E., Garde, A.A., Münker, C., 2017. Hafnium isotope constraints on the origin of Mesoarchaean andesites in southern West Greenland, North Atlantic craton. In: Halla, J., Whitehouse, M.J., Ahmad, T., Bagai, Z. (Eds.), Crust–Mantle Interactions and Granitoid Diversification: Insights from Archaean Cratons, vol. 449. Geological Society, London, Special Publications, pp. 19–38. http://dx.doi.org/10.1144/SP449.2.
Szilas, K., van Hinsberg, V.J., McDonald, I., Morishita, T., Pearson, D.G., 2016b. Highly Depleted Peridotites Within Mesoarchaean Orthogneiss at the Seqi Olivine Mine, SW Greenland – Potential Implications for the Formation of Cratonic Keels. Goldschmidt Conference, Abstract 3009, Yokohama. http://goldschmidt.info/2016/uploads/abstracts/finalPDFs/3009.pdf.
Terentiev, R.A., Savko, K.A., Santosh, M., 2016. Paleoproterozoic crustal evolution in the East Sarmatian Orogen: petrology, geochemistry, Sr–Nd isotopes and zircon U–Pb geochronology of andesites from the Voronezh massif, Western Russia. Lithos 246, 61–80.
Thakurta, J., Ripley, E.M., Li, C., 2008. Geochemical constraints on the origin of sulfide mineralization in the Duke Island Complex, southeastern Alaska. Geochemistry Geophysics Geosystems 9, Q07003.
Tiepolo, M., Oberti, R., Zanetti, A., Vannucci, R., Foley, S.F., 2007. Trace-element partitioning between amphibole and silicate melt. Reviews in Mineralogy and Geochemistry 67, 417–452.
Wager, L.R., Brown, G.M., Wadsworth, W.J., 1960. Types of igneous cumulates. Journal of Petrology 1, 73–85.
Wan, Z., Coogan, L.A., Canil, D., 2008. Experimental calibration of aluminum partitioning between olivine and spinel as a geothermometer. American Mineralogist 93, 1142–1147.
Wang, H., van Hunen, J., Pearson, D.G., 2016. Making Archean cratonic roots by lateral compression: a two-stage thickening and stabilization model. Tectonophysics (in press).
Warren, J.M., 2016. Global variations in abyssal peridotite compositions. Lithos 248–251, 193–219.
Witt-Eickschen, G., Seck, H.A., 1991. Solubility of Ca and Al in orthopyroxene from spinel peridotite: an improved version of an empirical geothermometer. Contributions to Mineralogy and Petrology 106, 431–439.
Wittig, N., Pearson, D.G., Webb, M., Ottley, C.J., Irvine, G.J., Kopylova, M., Jensen, S.M., Nowell, G.M., 2008. Origin of cratonic lithospheric mantle roots: a geochemical study of peridotites from the North Atlantic Craton, West Greenland. Earth and Planetary Science Letters 274, 24–33.
Wittig, N., Pearson, D.G., Baker, J.A., Duggen, S., Hoernle, K., 2010. A major element, PGE and Re–Os isotope study of Middle Atlas (Morocco) peridotite xenoliths: evidence for coupled introduction of metasomatic sulphides and clinopyroxene. Lithos 115, 15–26.
Wooden, J.L., Czamanske, G.K., Zientek, M.L., 1991. A lead isotopic study of the Stillwater Complex, Montana: constraints on crustal contamination and source regions. Contributions to Mineralogy and Petrology 107, 80–93.
WSU, 2016. Washington State University GeoAnalytical Lab. Technical Notes Describing Sample Preparation, Analytical Procedure, Precision, and Accuracy of XRF and ICP-MS Analysis can be Found at This Link. http://environment.wsu.edu/facilities/geolab/technotes.
Zhao, G., Wilde, S.A., Li, S., Sun, M., Grant, M.L., Li, X., 2007. U–Pb zircon age constraints on the Dongwanzi ultramafic–mafic body, North China, confirm it is not an Archean ophiolite. Earth and Planetary Science Letters 255, 85–93.
Zientek, M.L., 2012. Magmatic ore deposits in layered intrusions-Descriptive model for reef-type PGE and contact-type Cu-Ni-PGE deposits (No. 2012–1010). US Geological Survey.